This is a repository copy of *Rapid biotic rebound during the late Griesbachian indicates heterogeneous recovery patterns after the Permian-Triassic mass extinction*.

White Rose Research Online URL for this paper:
http://eprints.whiterose.ac.uk/138641/

Version: Accepted Version

Article:

1 # Rapid biotic rebound during the late Griesbachian

2 ## indicates heterogeneous recovery patterns after the

3 ## Permian-Triassic mass extinction

4

5 **Xu Dai[1], Haijun Song[1*], Paul B. Wignall[2], Enhao Jia[1], Ruoyu Bai[1], Fengyu**

6 **Wang[1], Jing Chen[3], Li Tian[1]**

7 *[1]State Key Laboratory of Biogeology and Environmental Geology, School of Earth*

8 *Sciences, China University of Geosciences, Wuhan 430074, China*

9 *[2]School of Earth and Environment, University of Leeds, Leeds LS2 9JT, UK*

10 *[3]Yifu Museum of China University of Geosciences, Wuhan 430074, China*

11 *Corresponding author. Email: haijun.song@aliyun.com

12 **ABSTRACT**

13 New fossil data of two Early Triassic (Griesbachian to Dienerian) sections from

14 South China show unusually high levels of both benthic and nektonic taxonomic

15 richness, occurring in the late Griesbachian. A total of 68 species (including 26 species

16 of Triassic-type species) representing mollusks, brachiopods, foraminifers, conodonts,

17 ostracods, and echinoderms occur in the late Griesbachian, indicating well-established

18 and relatively complex marine communities. Furthermore, the nekton shows higher

19 origination rates than the benthos. Analyses of sedimentary facies and size distribution

20 of pyrite framboids show that this high-diversity interval is associated with well-

21 oxygenated environments. In contrast to the previously suggested scenario that

22 persistently harsh environmental conditions impeded the biotic recovery during the

23   Early Triassic, our new findings, combined with recent works, indicate a fitful regional

24   recovery pattern after the Permian-Triassic crisis resulting in three main diversity highs:

25   late Griesbachian-early Dienerian, early-middle Smithian and Spathian. The transient

26   rebound episodes are therefore influenced by both extrinsic local (e.g. redox condition,

27   temperature) and intrinsic (e.g. biological tolerances, origination rate) parameters.

28   **INTRODUCTION**

29   The Permian-Triassic mass extinction (PTME) was the largest biotic catastrophe

30   of the Phanerozoic, which eliminated around 80% to 90% of marine species (Raup,

31   1979; Song et al., 2013; Stanley, 2016) and heralded the development of modern

32   ecosystems (Sepkoski, 1981; Brayard et al., 2017). After this mass extinction,

33   depauperate faunas were prevailed throughout the Early Triassic, and not until the

34   Middle Triassic did diversity rebound (Erwin and Pan, 1996; Nützel, 2005; Payne et al.,

35   2006; Tong et al., 2007). The delay has been attributed to the magnitude of the PTME

36   and the evolution to replace the losses (e.g. Erwin, 2001). Alternatively, persistent

37   environmental disturbances in the Early Triassic have been held responsible such as

38   marine anoxia (Algeo et al., 2007, 2008; Bond and Wignall, 2010; Song et al., 2012;

39   Tian et al., 2014; Clarkson et al., 2016; Lau et al., 2016; Wignall et al., 2016), high

40   temperatures (Sun et al., 2012; Romano et al., 2013), elevated atmospheric CO_2 (Fraiser

41   and Bottjer, 2007), and abnormal productivity (Algeo et al., 2011; Meyer et al., 2011;

42   Grasby et al., 2016). Additionally, the 'Lilliput effect' (dwarfism of surviving organisms)

43   was also pervasive among many clades during the Early Triassic, e.g. foraminifers

44   (Payne et al., 2011; Song et al., 2011), ostracods (Chu et al., 2015), bivalves (Twitchett,

45 2007), gastropods (Payne, 2005), and brachiopods (He et al., 2015). However, the

46 spatiotemporal extent and significance of this phenomenon are debated (see e.g.,

47 Brayard et al., 2010, 2015; Forel and Crasquin, 2015).

48   Contrary to the prolonged recovery scenario, recent studies on conodonts,

49 ammonoids and foraminifers reveal a fitful recovery pattern that shows diversification

50 was not underway until the Smithian (Orchard, 2007; Brayard et al., 2009; Song et al.,

51 2011), less than ~1.5 million years after the PTME. Recovery was then setback by a

52 severe crisis in the late Smithian (Brayard et al., 2006; Stanley, 2009). Data from Oman

53 (Krystyn et al., 2003; Twitchett et al., 2004), Italy (Hofmann et al., 2011, 2015; Foster

54 et al., 2017), the Northern Indian Margin (Brühwiler et al., 2010; Wasmer et al., 2012;

55 Kaim et al., 2013; Ware et al., 2015;), South Primorye (Shigeta et al., 2009), western

56 USA (Brayard et al., 2013, 2015, 2017; Hautmann et al., 2013; Hofmann et al., 2013,

57 2014), South China (Chen et al., 2007; Brayard and Bucher, 2008; Kaim et al., 2010;

58 Hautmann et al., 2011; 2015; Wang et al., 2017), and Svalbard (Foster et al., 2016) also

59 documented spatiotemporally variable diversification and occurrences of rather

60 complex communities. However, few of these works provide exhaustive correlation

61 between paleontological and environmental data to decipher the recovery course and

62 its controlling factors. In many regions, marine environments were apparently

63 depauperate during the Griesbachian-Dienerian with local exceptions (e.g. Twitchett et

64 al., 2004). Such occurrences are considered to have become more common in the

65 Spathian (Pietsch and Bottjer, 2014). Thus, the overall spatiotemporal pattern and the

66 clade variability of the biotic recovery following the PTME are still unclear and

67   therefore controversial, as well its environmental drivers.

68   Sampling efforts and preservation biases influence our knowledge of the biotic

69   recovery. For instance, Early Triassic silicified fossil assemblages are quite rare, but

70   show relatively high diversity when present (Foster et al., 2016). Extensive sampling

71   efforts and new findings might change our understanding of biotic recovery model (e.g.

72   Brayard et al., 2015, 2017). So far, no hypothesis has addressed the question of why the

73   re-diversification of a few clades (e.g. ammonoids and conodonts) were more rapid,

74   while others were rather slow (e.g. brachiopods). Recent studies showed that

75   environmental conditions (e.g. temperature, oxygen concentration) strongly fluctuated

76   in the Early Triassic (Algeo et al., 2011; Song et al, 2012; Sun et al, 2012; Grasby et al.,

77   2013; Tian et al., 2014), but only rarely have studies tried to link such environmental

78   fluctuations to observed recovery patterns amongst clades (e.g. Pietsch et al. 2014).

79   South China provides one of the best marine fossil records of the Permian-Triassic

80   transition, and often serves as an example of the prolonged recovery scenario (e.g.,

81   Payne et al., 2006; Tong et al., 2007). However, recent reports of unusually diverse

82   earliest Triassic faunas from Guangxi (Kaim et al. 2010; Hautmann et al. 2011) question

83   this model. Here we provide new paleontological and paleoenvironmental data from

84   two Griesbachian-Dienerian sections in Guizhou and Hubei provinces, South China,

85   that record relatively high diversity levels among several groups and their associated

86   paleoenvironmental indicators as potential biotic change drivers.

87   **GEOLOGICAL SETTING**

88   During the Early Triassic, the South China Block was located in equatorial

89   latitudes, at the interface between Panthalassa and Tethys (Fig. 1A). Marine Lower

90   Triassic sediments are widespread especially the carbonates of the Yangtze Platform.

91   This platform was located centrally in the South China Block, and adjacent to the

92   Nanpanjiang Basin (Fig. 1B). The platform successions are divided into the Daye

93   Formation, dominated by limestones, and the overlying Jialingjiang Formation,

94   composed of dolomites (Feng et al., 1997). Lower Triassic strata of the Nanpanjiang

95   Basin consists of basinal clastic and carbonate rocks plus shallower carbonates of

96   limited area which formed on isolated platforms (Feng et al., 1997; Bagherpour et al.,

97   2017). The two studied sections (Gujiao and Jianzishan) were located at the southern

98   and northern sides of the Yangtze Platform margin, respectively (Fig. 1B).

99   **Gujiao section**

100   The Gujiao section (26º30′49.22″N, 106º52′15.17″E) is located ~20 km east from

101   Guiyang and was situated in the transitional zone between the Nanpanjiang Basin and

102   the Yangtze Platform during the Early Triassic (Fig. 1B). A new and well-exposed

103   outcrop was found in 2015 along a newly-built road, close to the Gujiao County,

104   showing a continuous Permian-Triassic succession (Fig. 2A). The Upper Permian

105   Changxing Formation is dominated by light gray, bioclastic limestones, and yields

106   abundant and diverse Permian organisms including brachiopods, gastropods, corals,

107   dasycladacean algae, and foraminifers. The overlying Dalong Formation consists of

108   cherty mudstones and black shales, with occasionally volcanic ash beds, representing a

109   deeper basinal environment. The Dalong Formation contains abundant radiolarian

110   (Feng and Algeo, 2014; Xiao et al., 2017) and ammonoid (Zheng, 1981) faunas that

111 indicate a late Changhsingian age. The Lower Triassic Daye Formation conformably

112 overlies the Dalong Formation, and is dominated by marlstones alternating with shales

113 (Fig. 2B, C). The Permian-Triassic boundary is roughly correlated with the boundary

114 between the Dalong and Daye formations. Ammonoids are very abundant in the lower

115 part of Daye Formation. Dai et al. (submitted) identified three ammonoid beds in this

116 interval, the late Griesbachian *Ophiceras medium* and *Jieshaniceras guizhouense* beds,

117 and the middle Dienerian *Ambites radiatus* bed. The exact position of the

118 Griesbachian/Dienerian boundary is not well defined at Gujiao, but is likely just above

119 the *Jieshaniceras guizhouense* beds.

120 **Jianzishan section**

121 The Jianzishan (30º9′58.08″N, 109º0′27.5″E) section found ~20 km south of

122 Lichuan in Hubei Province, was located on the north margin of the Yangtze Platform

123 (Fig. 1B). The Late Permian and Early Triassic are represented by the Changxing and

124 Daye formations respectively. The former consists of thick-bedded bioclastic

125 limestones and calcareous sponge reefs with associated shallow-marine fossils (e.g.

126 corals, calcareous algae and fusulinids). The diverse fauna includes nautiloids,

127 foraminifers, dasycladacean algae, sponges, corals, and brachiopods (Liu et al., 2017).

128 The lowermost part of the Daye Formation is a 2.4 m thick microbialite (Fig. 2D), a

129 typical representative of the extensive microbial deposits found in the lowermost

130 Triassic strata of South China (e.g. Lehrman, 1999; Yang et al., 2011; Bagherpour et al.,

131 2017). The overlying strata are dominated by alternations of thin-bedded marlstones

132 and shales (Fig. 2E) that yield abundant bivalves, brachiopods (Wang et al., 2017) and

133   ammonoids, suggestive of an outer platform facies. Two ammonoid beds, the late

134   Griesbachian *Ophiceras* sp. indet. and *Jieshaniceras guizhouense* beds are known (Bai

135   et al., 2017). Four conodont zones, the late Changhsingian *Clarkina changxingensis*

136   Zone and *Clarkina yini* Zone, the Griesbachian *Hindeodus parvus* Zone and the

137   *Hindeodus postparvus* Zone, were found in the Jianzishan section (Bai et al., 2017).

138   Strata between the *H. parvus* and the *H. postparvus* zones are not well dated by

139   conodonts or ammonoids. Consequently, we here use the presence of abundant

140   *Sinolingularia* to denote the assemblage at this level.

141   **MATERIAL AND METHODS**

142   Macrofossils (e.g., ammonoids and bivalves) were collected by mechanically

143   breaking up decimeter-sized blocks. Mechanical techniques, including air and electrical

144   scribes, were later performed in the laboratory to excavate morphologic details and

145   thereby facilitate species-level identification. Specimens were photographed using a

146   Canon 70D camera with a Micro lens EF 100mm f/2.8.

147   A total of 39 and 38 thin sections have been made to study microfossils from the

148   Gujiao and Jianzishan sections, respectively. In addition, 16 and 18 samples were

149   respectively collected from the Gujiao and Jianzishan sections for analyses of the size

150   distribution of pyrite framboids. A polished slab (~1 × 1 cm) of each sample was

151   examined for size measurements of pyrite framboids using a Scanning Electronic

152   Microscope (SEM; Hitachi SU8000) at the State Key Laboratory of Biogeology and

153   Environmental Geology in Wuhan, China. Paleoenvironmental factors have been

154   investigated including local redox conditions determined using pyrite framboid size

155 analysis, following the approach of Bond and Wignall (2010). A minimum of 100 pyrite

156 framboids were measured when possible, according to the procedure of Huang et al.,

157 (2017).

158 **PALEONTOLOGICAL RESULTS**

159 Over 3500 specimens were collected from the Gujiao and Jianzishan sections (Figs

160 3, 4, Tables 1, 2), including ammonoids, nautiloids, bivalves, gastropods, brachiopods,

161 ostracods, echinoids, foraminifers, and conodonts. Paleozoic holdover and new

162 originated genus and species (species that belongs to new originated genus)   are used

163 to qualitatively assess the composition of the biotas.

164 **Ammonoids**

165 Thirteen ammonoid species occur in the lower Daye Formation at the Gujiao

166 section, and seven ammonoid species occur in the lower Daye Formation from the

167 Jianzishan section (Bai et al., 2017). All ammonoid taxa from the two sections are new

168 originated. At Gujiao, five species (*Ophiceras medium*, Ophiceratidae gen. indet.,

169 Gyronitidae gen. indet., *Vishnuites pralambha* and ?Mullericeratidae gen. indet.) were

170 found in the *Ophiceras medium* beds. Five species (*Vishnuites pralambha, Ophiceras*

171 sp. indet., *Mullericeras* sp. nov., *Jieshaniceras guizhouense* and *Proptychites* sp. indet.)

172 were identified in the *Jieshaniceras guizhouense* beds. Four species (*Ambites radiatus,*

173 *Pseudoproptychites* cf. *hiemalis,* ?Gyronitidae gen et sp. nov and ?*Ussuridiscus* cf.

174 *varaha*) occur in the *Ambites radiatus* bed. At Jianzishan, only one taxon was found in

175 the *Ophiceras* sp. indet. beds. Six species (*Vishnuites pralambha, Ussuridiscus varaha,*

176 *Jieshaniceras guizhouense*, ?Gyronitidae gen. et sp. nov, *Hubeitoceras yanjiaensis* and

177   *Shangganites* sp. indet.) occur in the *Jieshaniceras guizhouense* beds.

178   Two successive ammonoid diversity levels are thus obvious: 1) a relatively high

179 species richness during the late Griesbachian, and 2) a relatively low species richness

180 level in the middle Dienerian, with a minimum richness above that. At Jianzishan, no

181 ammonoids were found in strata overlying the *Jieshaniceras guizhouense* beds.

182 **Nautiloids**

183   Nautiloids show a weak diversity level during the late Griesbachian (Fig. 5). Two

184 new originated nautiloids (*Xiaohenautilus huananensis* and *X. sinensis*) were identified

185 in the *Ophiceras medium* and *Jieshaniceras guizhouense* beds at the Jianzishan section.

186 Except for these two species, an unidentified nautiloid was also found in the

187 *Jieshaniceras guizhouense* beds at the Gujiao section. It mainly differs from

188 *Xiaohenautilus* by marked ribs on its flanks (Fig. 5). *X. huananensis* and *X. sinensis*

189 also occur in the *Jieshaniceras guizhouense* beds at Jianzishan.

190 **Bivalves**

191   At Gujiao, only three beds yield well preserved bivalves. A bed ~ 20 cm below the

192 middle Dienerian *Ambites radiatus* bed shows abundant bivalves identified as *Claraia*

193 *stachei*. The *Ambites radiatus* bed contains moderately abundant *Claraia radialis*, and

194 the overlying beds have abundant *Claraia aurita* (Fig. 6). These three *Claraia* species

195 belong to Paleozoic holdovers.

196   Seven bivalve species were found at Jianzishan (Figs. 6, 7): three species (*Claraia*

197 sp. indet., *Claraia wangi* and *Eumorphotis venetiana*) in the *Sinolingularia* beds, six

198 species (*C. wangi*, *C. zhenanica*, *E. venetiana*, *Eumorphotis* sp. indet., *Pteria ussurica*

199 *variabilis*, and *Scythentolium scutigerulus*) in the *Ophiceras* sp. indet. beds and two

200 species (*C.* sp. indet. and *C. zhenanica*) in the *Jieshaniceras guizhouense* beds. Three

201 of the species are new originated: *Eumorphotis venetiana*, *Eumorphotis* sp. indet. and

202 *Scythentolium scutigerulus*. The *Ophiceras* sp. indet. beds contain the most diverse and

203 abundant bivalves.

204 **Gastropods**

205   Gastropods specimens are poorly preserved at both sections (Fig. 8). Thus, their

206 taxonomic assignment is often tentative. Identifications were mainly based on their

207 shell height and width, and number of whorls. We also categorized studied specimens

208 under the following designation 'unidentified gastropod A, B, C, etc'. to distinguish

209 them when necessary.

210   At least seven species are present at Jianzishan, two (Bellerophontidae gen. indet.

211 and unidentified gastropod A) in the *Hindeodus parvus* Zone, one (Bellerophontidae

212 gen. indet.) in the *Sinolingularia* beds, two (Bellerophontidae gen. indet.

213 and ?*Pseudomurchisonia* sp. indet) in the *Ophiceras* sp. indet. beds and three

214 (unidentified gastropods A, B and C) in the *Jieshaniceras guizhouense* beds.

215   At Gujiao, four gastropods species were found, three (?*Naticopsis* sp. indet.,

216 unidentified gastropods D, E) in the *Ophiceras medium* beds, four (?*Naticopsis* sp.

217 indet., Bellerophontidae gen. indet. and unidentified gastropods D, E) in the

218 *Jieshaniceras guizhouense* beds, and one (unidentified gastropod E) in the *Ambites*

219 *radiatus* bed. Gastropods are absent in the overlying beds. In summary, gastropods are

220 abundant in the late Griesbachian *Ophiceras medium* and *Jieshaniceras guizhouense*

221   beds, but seemingly displaya low diversity.

Brachiopods

223   Only one brachiopod species (*Lichuanorelloide lichuanensis*) was excavated from

224   the *Jeshaniceras guizhouense* beds at Gujiao, whilst five brachiopods species

225   (including three articulated brachiopods) were recognized at Jianzishan. *Sinolingularia*

226   sp. indet. is very abundant in the *Sinolingularia* beds (Fig. 7). The *Ophiceras* sp. indet.

227   beds contain two brachiopods species (*Crurithyris* sp. indet. and *Lingularia* sp. indet.,

228   Fig. 7) and the *Jeshaniceras guizhouense* beds have a relatively diverse brachiopod

229   fauna with five identified species (*Sinolingularia* sp. indet., *Lingularia* sp. indet.,

230   *Crurithyris* sp. indet., *Lichuanorelloide lichuanensis* and *Lissorhynchia* sp. indet.).

231   Among these five species, three (*Sinolingularia* sp. indet., *Lichuanorelloide*

232   *lichuanensis* and *Lissorhynchia* sp. indet.) are new originated, and suggest a notable

233   brachiopod diversification after the PTME (Wang et al., 2017).

Foraminifers

235   A total of 20 species were identified in the Gujiao and Jianzishan sections (Fig. 9).

236   At Gujiao, seven species (*Nodosinelloides* sp. indet., *Gaudryina* sp. indet., *Dentalina*

237   sp. indet., *Tolypammina* sp. indet., *Glomospira* sp. indet., *Duotaxis* sp. indet.

238   and ?*Dagmarita* sp. indet.) occur in the *Ophiceras medium* beds, and ten

239   (*Nodosinelloides* sp. indet., *Gaudryina* sp. indet., *Dentalina* sp. indet., *Tolypammina* sp.

240   indet., *Glomospira* sp. indet., *Duotaxis* sp. indet., ?*Dagmarita* sp. indet., *Geinitzina* sp.

241   indet., ?*Vervilleina* sp. indet. and *Nodosaria* sp. indet.) in the *Jeshaniceras guizhouense*

242   beds. Two species are new originated, *Gaudryina* sp. indet. and *Duotaxis* sp. indet.

243 Overall, foraminiferal species richness was relatively high during the late Griesbachian,

244 whereas no foraminifer specimens were retrieved from the overlying Dienerian strata.

245   At Jianzishan, 12 species (*Earlandia* sp. indet., *Postcladella kalhori*, *Ammodiscus*

246 sp. indet., *Dentalina* sp. indet., "*Nodosaria*" sp. indet., *Tezaquina* sp. indet.,

247 *Heimigordius* sp. indet., *Nodosinelloides* sp. indet., ?*Duotaxis* sp. indet., *Geinitzina* sp.

248 indet., "*Nodosaria*" *elabugae* and "*Nodosaria*" *skyphica*) were found in the *Hindeodus*

249 *parvus* Zone, but no foraminifer specimens were found in the *Sinolingularia* beds and

250 *Ophiceras* sp. indet. beds. Eight species (*Postcladella kalhori*, *Nodosinelloides* sp.

251 indet., *Geinitzina* sp. indet., *Glomospira* sp. indet., *Tolypammina* sp. indet., *Frondina*

252 sp. indet., *Vervilleina* sp. indet. and *Nodosinelloides sagitta*) occur in the *Jieshaniceras*

253 *guizhouense* beds. All these species belong to Paleozoic holdovers.

254 **PYRITE FRAMBOID RESULT AND PALEOREDOX INTERPRETATION.**

255 **Gujiao section**

256   At Gujiao, five of the 16 samples exhibit abundant framboids, whereas the rest

257 contained few or no pyrite framboids (Fig. 10). Framboids in samples GJ-f and GJ-11

258 display a small mean diameter (3.15 μm and 4.76 μm respectively), as well as small

259 standard deviations (1.14 and 2.66 respectively; Fig. 11). These measurements suggest

260 euxinic-anoxic conditions for these beds (Fig. 12), based on the approach of Bond and

261 Wignall (2010) and Tian et al. (2014). Nine samples from the *Ophiceras medium* and

262 *Jieshaniceras guizhouense* beds yield few or no framboids. Three of the remaining six

263 samples from the overlying Dienerian strata show occurrences of framboids (Fig. 10).

264 Only one sample, (GJ-40) from the *Ambites radiatus* bed, is dominated by small

265　framboids, with a small mean diameter and standard deviation (MD = 4.76 μm, SD =

266　1.98; Fig. 11), indicating euxinic-anoxic condition (Fig. 12). Above this bed, two

267　samples (GJ-III-5+0.2 and GJ-III-5+0.9) yield abundant framboids, with a larger mean

268　diameter, about 5.8 μm (Fig. 11). These plot in the weakly dysoxic (GJ-III-5+0.2) and

269　anoxic fields (GJ-III-5+0.9) in figure 12 which is calibrated from studies of modern

270　environments that record a range of redox-related regimes (Bond and Wignall, 2010).

271　　The paleoredox trends derived from pyrite framboid size distributions are

272　congruent with occurrences of trace fossils and the observed succession of facies (Figs

273　2, 13). Anoxic and dysoxic intervals, inferred from framboid data, coincide with an

274　absence of bioturbation and correspond to dark, thin-bedded, finely laminated

275　marlstones interbedded with black shales (Fig. 2B). The beds with rare or no pyrite

276　framboids are dominated by light-gray, thin bedded marlstones (Fig. 2C) with abundant

277　vertical tracers *Arenicolites* (Fig. 13A).

278　**Jianzishan section**

279　　At Jianzishan, only two samples (JZS-2+1.1 and JZS-2+2.1) from the basal

280　Triassic microbialites yield moderately abundant, large pyrite framboids, whereas

281　framboids were rare or absent in other samples (Fig. 10). Both framboid populations

282　exhibit diameters and standard deviations that plot in dysoxic fields (Fig. 12). Other

283　samples lack pyrite framboids and likely indicate oxic conditions during deposition of

284　the *Sinolingularia, Ophiceras* sp. indet. and *Jieshaniceras guizhouense* beds.

285　Moderately abundant vertical ichnofossils (e.g. *Skolithos*) occur in the *Jieshaniceras*

286　*guizhouense* beds (Fig. 13B), also suggesting well-oxygenated conditions.

287   **DISCUSSION**

288   **Late Griesbachian rapid recovery**

289   Previous works in South China support the claims of a delayed recovery in China

290   caused by persisting environmental stresses up until at least the Spathian (e.g. Payne et

291   al., 2006; Tong et al., 2007; Sun et al., 2012; Song et al., 2012). Chen et al. (2007)

292   documented a rapid onset of recovery at Meishan section, however, only nine species

293   of macrofossils were found during late Griesbachian. Our data show that moderately

294   diverse marine communities flourished soon after the PTME, during the late

295   Griesbachian, at least in well-oxygenated environments. Rarefaction analyses indicate

296   that the highest diversity is in the *Jieshaniceras guizhouense* beds both at Gujiao and

297   Jianzishan (Fig. 14). Furthermore, the microbialite community (early Griesbachian) is

298   rather diverse at Jianzishan that likely results from the non-lethal oxygen poor

299   conditions and supports the microbialites refuge model (Forel et al., 2013). At Gujiao,

300   the early Griesbachian witnessed depressed marine community under anoxic-euxinic

301   conditions in the aftermath of PTME. The diversity in the *Jieshaniceras guizhouense*

302   beds at Gujiao is lower than that at Jianzishan, 26 and 37 species at Gujiao and

303   Jianzishan respectively, supporting that redox condition plays a significant role in

304   diversity rebound. There is no marked shift in facies observed near the

305   Griesbachian/Dienerian boundary at the both sections indicating that the dramatic

306   diversity reduction after the late Griesbachian is not a bias resulting from major facies

307   change. However, the causation of this small crisis still needs more work to decipher.

308   At Jianzishan, a marked Paleozoic holdovers diversity drop is observed between

309   the *Hindeodus parvus* Zone and *Sinolingularia* beds (Figs 4, 15), possibly reflecting

310   the second pulse of the PTME in the earliest Triassic mass extinction (Song et al., 2013).

311   Alternatively (or additionally), this diversity loss might be related to the facies shift

312   between the microbialites and mudstones (Fig. 4). High diversity levels of Paleozoic

313   holdovers and new originated taxa occurred during the late Griesbachian in both

314   sections. Additionally, during the late Griesbachian, nektonic taxa show a more marked

315   rebound than benthic organisms, e.g. ammonoid (proptychitids). This difference

316   between nektonic and benthic taxa may result from the relatively stronger mobility of

317   nektonic organisms such as cephalopods, which makes them better able to avoid

318   spatially variable hostile environments (Bambach et al., 2002). However, it could also

319   reflect the intrinsically evolutionary rate of ammonoids that tends to be high, compared

320   to other mollusk groups, at all times during the clades' history (Stanley, 2009).

321   Well-oxygenated conditions during the late Griesbachian have rarely been

322   documented in South China, and the interval is widely reported to be poorly ventilated

323   in marine settings (Song et al., 2012; Tian et al., 2014; Huang et al., 2017; Li et al.,

324   2016). Our data reveal that there were heterogeneous redox conditions at this time.

325   Gujiao and Jianzishan sections were located on the platform margin, a predicted

326   "Refuge Zone" sandwiched beneath the potentially warm surface waters and anoxic

327   deeper waters (Song et al. 2014; Godbold et al., 2017). Our results suggest that diversity

328   patterns in the Early Triassic were strongly controlled by the presence of anoxia, with

329   recovery best seen in the limited areas of more ventilated conditions (Fig. 15).

330   Similar high diversity levels rapidly after the PTME are also known from a limited

331 number of other locations. For example, a late Griesbachian fauna with ammonoids,

332 bivalves and gastropods in oxic strata is seen in Oman (Krystyn et al., 2003; Twitchett

333 et al., 2004). The overall diversity during Griesbachian and Dienerian at Meishan

334 section is relative high, probably owing to its overmuch studies, especially near the

335 Permian-Triassic boundary. In addition, the diverse conodont fauna contributes the

336 most of overall diversity (Zhang et al., 2007). However, the low diversity of mollusk

337 taxa and oxygen poor conditions during the late Griesbachian at Meishan also support

338 that redox condition is a key factor in controlling biotic recovery (Chen et al., 2007,

339 2014; Li et al., 2016). The Siusi Member (late Griesbachian-Dienerian) of the Werfen

340 Formation (Dolomites, Italy) also yields relatively diverse mollusk communities in well

341 oxygenated environment (Wignall and Twitchett, 1996; Hofmann et al., 2015; Foster et

342 al., 2017). A marked ammonoid diversity richness has been documented in the Northern

343 Indian Margin (Salt Range and Spiti) during the early Dienerian (Ware et al., 2015),

344 and this interval was proved to be well oxygenated (Hermann et al., 2011). Combination

345 of the works above and present work support the heterogeneous recovery pattern and

346 rapid diversification only present under oxic conditions.

347 Several studies described diverse mollusk faunas from the earliest Triassic

348 microbialites of South China (Kaim et al., 2010; Hautmann et al., 2011, 2015). The

349 microbialites may have serve as a refuge for benthic organisms (e.g., Forel et al., 2013),

350 but reconstructions of paleoredox conditions within these deposits suggests variety of

351 redox conditions (e.g. Forel et al., 2009, 2013; Liao et al., 2017). However, these

352 microbialites occur between the two phases of the PTME (Jiang et al., 2014; Brosse et

353   al., 2015) that straddle the Permian-Triassic boundary (Song et al., 2013), and thus

354   record intra-extinction conditions not those during the recovery. It is noteworthy that

355   the most microbialite taxa are Paleozoic holdovers (Hautmann et al., 2015), and so just

356   record assemblages that survived the first (but not the second) stage of the PTME.

357   In South China, biotic recovery was impeded by anoxic events later in the

358   Dienerian (Figs. 10, 15), as also seen in other basins, e.g. Pakistan (Hermann et al.,

359   2011) and northern Italy (Foster et al., 2017). Overall, previous works and our results

360   suggest that recovery after the PTME was spatiotemporally heterogeneous and highly

361   dependent on local environmental conditions as seen during the late Griesbachian in

362   our two studied sections with same sample effort and similar preservation conditions in

363   South China. The most abundant and diversified Griesbachian communities were to be

364   in shallower (but not the shallowest) and more oxic settings.

365   **Fitful recovery pattern**

366   Based on our new data and previous studies, a fitful recovery pattern from the

367   PTME can be simplified into three distinct phases of relatively high diversity that vary

368   in time and space according to regional and local environmental conditions: I. late

369   Griesbachian-early Dienerian; II. early-middle Smithian and III. Spathian. During

370   phase I, new originated genus became the dominant group in South China, especially

371   amongst the ammonoid-dominated nektonic communities. This recovery phase was

372   short-lived and probably curtailed by the return of anoxic conditions during the

373   Dienerian. Phase II during the early-middle Smithian is well documented by further

374   recovery seen among ammonoids (Brayard et al., 2009; Brühwiler et al., 2010),

conodonts (Orchard, 2007) and foraminifers (Song et al., 2011). This time interval also witnessed the local development of rather diverse community (Haig et al., 2015) and sponge bioconstructions (Brayard et al., 2011) and the presence of large-sized organisms (Brayard et al., 2010, 2015). It was associated with a relatively cooling interval (Sun et al., 2012; Romano et al., 2013) and well-oxygenated conditions (Galfetti et al., 2008; Grasby et al., 2013). This phase of diversification was followed by a severe extinction in the late Smithian (Orchard, 2007; Brayard et al., 2009; Stanley, 2009), seemingly related to high temperatures and anoxia (Sun et al., 2012; Song et al., 2012; Grasby et al., 2013). At that time, foraminifers only show a diversity low point, but no real extinction (Song et al., 2011). The Phase III diversification occurred rapidly after the late Smithian event and is seen among both nektonic and benthic forms (Brayard et al., 2009, 2017; Stanley, 2009; Song et al, 2011; Chen et al, 2015; Hautmann et al., 2013). It also witnessed the appearance of top-level predators in the fossil record (e.g. Scheyer et al. 2014; Motani et al., 2015). The Phase III diversification is associated with a cooling trend (Sun et al., 2012; Romano et al., 2013) and with the end of anoxic events characterized by the widespread occurrence of marine red beds (Song et al., 2017).

As a whole, regional environmental fluctuations controlled the recovery in space and time. The fitful recovery model gets more and more strong evidences than delayed claims, at the same time, the deteriorative environment conditions are clarified to be recurrent (e.g. Sun et al., 2012; Song et al., 2012; Grasby et al., 2013; Huang et al., 2017). The differences between benthic and nektonic/pelagic organisms recovery

397 patterns and underlying processes are still unclear, but are probably related to

398 physiology variations (Bambach et al., 2002), intrinsic evolutionary rates (Stanley,

399 2009), and biological adaptation and competition rates (Hautmann et al., 2015). More

400 exhaustive integrated works (paleontological and environmental) within a high-time

401 resolution are necessary to decipher spatiotemporally heterogeneous recovery patterns

402 among different lineages.

403 **CONCLUSION**

404 New evidence from two sections in South China has revealed relatively high

405 diversity levels of ammonoids, bivalves, brachiopods, conodonts, foraminifers and

406 gastropods during the late Griesbachian. These high diversity levels are associated with

407 unusually well-oxygenated conditions for this period. The nektonic taxa show more

408 stronger diversity rebound than benthic forms, possibly due to their ecology (tiering,

409 stronger mobility) or evolutionary factors (ammonoids show much higher origination

410 rates than benthic mollusks (Brayard et al., 2009)). Our results show a spatiotemporally

411 heterogeneous recovery pattern linked to redox conditions, in both benthic and nektonic

412 communities in the investigated sections in South China. In contrast to the notion of

413 persistently harsh environmental conditions during the Early Triassic, our results

414 suggest that there was a regionally variable recovery pattern after the PTME, linked to

415 amelioration of environmental stresses, with three main high diversity phases during

416 the late Griesbachian-early Dienerian, early-middle Smithian and Spathian.

425 **REFERENCES CITED**

426 Algeo, T.J., Ellwood, B., Nguyen, T.K.T., Rowe, H., and Maynard, J.B., 2007, The

427 Permian-Triassic boundary at Nhi Tao, Vietnam: Evidence for recurrent influx of

428 sulfidic watermasses to a shallow-marine carbonate platform: Palaeogeography,

429 Palaeoclimatology, Palaeoecology, v. 252, p. 304–327,

430 doi:10.1016/j.palaeo.2006.11.055.

431 Algeo, T., Shen, Y., Zhang, T., Lyons, T., Bates, S., Rowe, H., and Nguyen, T.K.T., 2008,

432 Association of ^{34}S‐depleted pyrite layers with negative carbonate δ^{13}C excursions

433 at the Permian‐Triassic boundary: Evidence for upwelling of sulfidic deep‐

434 ocean water masses: Geochemistry, Geophysics, Geosystems, v. 9, no. 4, p. 1–10,

435 doi:10.1029/2007GC001823.

436 Algeo, T.J., Chen, Z.Q., Fraiser, M.L., and Twitchett, R.J., 2011, Terrestrial-marine

437 teleconnections in the collapse and rebuilding of Early Triassic marine ecosystems:

438 Palaeogeography, Palaeoclimatology, Palaeoecology v. 308, p. 1–11,

439 doi:10.1016/j.palaeo.2011.01.011.

440 Bagherpour, B., Bucher, H., Baud, A., Brosse, M., Vennemann, T., Martini, R., and

441   Guodun, K., 2017, Onset, development, and cessation of basal Early Triassic

442   microbialites (BETM) in the Nanpanjiang pull-apart Basin, South China

443   Block: Gondwana Research, v. 44, p. 178–204, doi:10.1016/j.gr.2016.11.013

444   (2016).

445 Bai, R., Dai, X., and Song, H., 2017, Conodont and ammonoid biostratigraphies around

446   the Permian-Triassic boundary from the Jianzishan of South China: Journal of

447   Earth Science, v. 28, no. 4, p. 595–613, doi:10.1007/s12583-017-0754-4.

448 Bambach, R.K., Knoll, A.H., and Sepkoski, J.J., 2002, Anatomical and ecological

449   constraints on Phanerozoic animal diversity in the marine realm: Proceedings of

450   the National Academy of Sciences, v. 99, no. 10, p. 6854–6859, doi:

451   10.1073/pnas.092150999.

452 Bond, D.P., and Wignall, P.B., 2010, Pyrite framboid study of marine Permian-Triassic

453   boundary sections: a complex anoxic event and its relationship to

454   contemporaneous mass extinction: Geological Society of America Bulletin, v. 122,

455   no. 7–8, p. 1265-1279, doi:10.1130/B30042.1.

456 Brayard, A., and Bucher, H., 2008, Smithian (Early Triassic) ammonoid faunas from

457   northwestern Guangxi (South China): taxonomy and biochronology: Fossils and

458   Strata, v. 55, p. 1–184.

459 Brayard, A., Escarguel, G., Bucher, H., Monnet, C., Brühwiler, T., Goudemand, N.,

460   Galfetti, T., and Guex, J., 2009, Good genes and good luck: ammonoid diversity

461   and the end-Permian mass extinction: Science, v. 325, no. 5944, p. 1118–1121,

462   doi:10.1126/science.1174638.

463   Brayard, A., Nützel, A., Stephen, D.A., Bylund, K.G., Jenks, J., and Bucher, H., 2010,

464   Gastropod evidence against the Early Triassic Lilliput effect: Geology, v. 38, no.

465   2, p. 147–150, doi:10.1130/G30553.1.

466   Brayard, A., Vennin, E., Olivier, N., Bylund, K.G., Jenks, J., Stephen, D.A., Bucher, H.,

467   Hofmann, R., Goudemand, N., and Escarguel, G., 2011, Transient metazoan reefs

468   in the aftermath of the end-Permian mass extinction: Nature Geoscience, v. 4, no.

469   10, p. 693–697, doi:10.1038/ngeo1264.

470   Brayard, A., Bylund, K.G., Jenks, J.F., Stephen, D.A., Olivier, N., Escarguel, G., Fara,

471   E., and Vennin, E., 2013, Smithian ammonoid faunas from Utah: implications for

472   Early Triassic biostratigraphy, correlation and basinal paleogeography: Swiss

473   Journal of Palaeontology, v. 132, no. 2, p. 141–219, doi: 10.1007/s13358-013-

474   0058-y.

475   Brayard, A., Meier, M., Escarguel, G., Fara, E., Nützel, A., Olivier, N., Bylund, K.G.,

476   Jenks, J. F., Stephen, D. A., Hautmann, M., Vennin, E., and Bucher, H., 2015, Early

477   Triassic Gulliver gastropods: Spatio-temporal distribution and significance for

478   biotic recovery after the end-Permian mass extinction: Earth-Science Reviews, v.

479   146, p. 31–64, doi:10.1016/j.earscirev.2015.03.005.

480   Brayard, A., Krumenacker, L.J., Botting, J.P., Jenks, J.F., Bylund, K.G., Fara, E.,

481   Vennin, E., Olivier, N., Goudemand, N., Saucede, T., Charbonnier, S., Romano,

482   C., Doguzhaeva, L., Thuy, B., Hautmann, M., Stephen, D.A., Thomazo, C., and

483   Escarguel, G., 2017, Unexpected Early Triassic marine ecosystem and the rise of

484   the Modern evolutionary fauna: Science Advances, v. 3, no. 2, p. e1602159, doi:

485   10.1126/sciadv.1602159.

486   Brönnimann, P., Zaninetti, L., and Bozorgnia, F., 1972, Triassic (Skythian) smaller

487   foraminifera from the Elika Formation of the central Alborz, northern Iran, and

488   from the Siusi Formation of the Dolomites, northern Italy: Mitteilung Gesellschaft

489   der Geologie und Bergsbaustudenten, Innsbruck, v. 21, p. 861-884.

490   Brosse, M., Bucher, H., Bagherpour, B., Baud, A., Frisk, Å. M., Guodun, K.,

491   Goudemand, N., and Hautmann, M., 2015, Conodonts from the Early Triassic

492   microbialite of Guangxi (South China): implications for the definition of the base

493   of the Triassic System: Palaeontology, v. 58, no. 3, p. 563–584, doi:

494   10.1111/pala.12162.

495   Brühwiler, T., Brayard, A., Bucher, H., and Guodun, K, 2008, Griesbachian and

496   Dienerian (Early Triassic) ammonoid faunas from northwestern Guangxi and

497   southern Guizhou (South China): Palaeontology, v. 51, no. 5, p. 1151–1180,

498   doi:10.1111/j.1475-4983.2008.00796.x.

499   Brühwiler, T., Bucher, H., Brayard, A., and Goudemand, N., 2010, High-resolution

500   biochronology and diversity dynamics of the Early Triassic ammonoid recovery:

501   The Smithian faunas of the Northern Indian Margin: Palaeogeography,

502   Palaeoclimatology, Palaeoecology, v. 297, no. 2, p. 491–501,

503   doi:10.1016/j.palaeo.2010.09.001.

504   Chen, J., Tong, J., Song, H., Luo, M., Huang, Y., and Xiang, Y., 2015, Recovery pattern

505   of brachiopods after the Permian-Triassic crisis in South China: Palaeogeography,

506   Palaeoclimatology, Palaeoecology, v. 433, p. 91–105,

507   doi:10.1016/j.palaeo.2015.05.020.

508 Chen, Z.Q., and Benton, M.J., 2012, The timing and pattern of biotic recovery

509   following the end-Permian mass extinction: Nature Geoscience, v. 5, no. 6, p. 375–

510   383, doi:10.1038/ngeo1475.

511 Chen, Z.Q., Tong, J., Kaiho, K., and Kawahata, H., 2007, Onset of biotic and

512   environmental recovery from the end-Permian mass extinction within 1–2 million

513   years: a case study of the Lower Triassic of the Meishan section, South

514   China: Palaeogeography, Palaeoclimatology, Palaeoecology, v. 252, no. 1, p. 176–

515   187, doi:10.1016/j.palaeo.2006.11.042.

516 Chen, Z. Q., Yang, H., Luo, M., Benton, M. J., Kaiho, K., Zhao, L., Huang, Y., Zhang,

517   K., Fang, Y., Jiang, H., Qiu, H., Li, Y., Tu, C., Shi, L., Zhang, L., Feng, X., and

518   Chen, L., 2015, Complete biotic and sedimentary records of the Permian–Triassic

519   transition from Meishan section, South China: ecologically assessing mass

520   extinction and its aftermath: Earth-science reviews, v. 149, p. 67-107,

521   doi:10.1016/j.earscirev.2014.10.005.

522 Cherdyntsev, W., 1914, Foraminiferal fauna of the Permian deposits of the eastern belt

523   of European Russia. Kazan: Trudy Obshchestva Estestvoispytateley pri

524   Imperatorskomy Kazanskomy Universitety v. 46, p. 3–88 (in Russian).

525 Chu, D., Tong, J., Song, H., Benton, M.J., Song, H., Yu, J., Qiu, X., Huang, Y., and Tian,

526   L., 2015, Lilliput effect in freshwater ostracods during the Permian–Triassic

527   extinction: Palaeogeography, Palaeoclimatology, Palaeoecology, v. 435, p. 38–52,

528   doi: 10.1016/j.palaeo.2015.06.003.

529 Clarkson, M. O., Wood, R. A., Poulton, S. W., Richoz, S., Newton, R. J., Kasemann, S.

530   A., Bowyer, F., and Krystyn, L., 2016, Dynamic anoxic ferruginous conditions

531   during the end-Permian mass extinction and recovery: Nature communications, v.

532   7, p. 12236, doi:10.1038/ncomms12236.

533   Efimova, N.A., 1974, Triassic foraminifers of the northwest Caucasus and Cis-

534   Caucasus: Akademiya Nauk SSSR, Voptosy Mikropaleontologii v. 17, p. 54–83

535   (in Russian, with English abstract).

536   Erwin, D.H., 2001, Lessons from the past: biotic recoveries from mass extinctions:

537   Proceedings of the National Academy of Sciences, v. 98, no. 10, p. 5399–5403,

538   doi: 10.1073/pnas.091092698.

539   Erwin, D.H., and Pan, H., 1996, Recoveries and Radiations: Gastropods After the

540   Permo-Triassic Mass Extinction: Geological Society, London, Special

541   Publications, v. 102, no. 1, p. 223–229, doi:10.1144/GSL.SP.1996.001.01.15.

542   Feng, Q., and Algeo, T.J., 2014, Evolution of oceanic redox conditions during the

543   Permo-Triassic transition: Evidence from deepwater radiolarian facies: Earth-

544   Science Reviews, v. 137, p. 34–51, doi: 10.1016/j.earscirev.2013.12.003.

545   Feng, Z., Bao, Z. and Liu, S. 1997. Lithofacies palaeogeography of Early and Middle

546   Triassic of South China. Beijing: Petroleum Industry Press.

547   Forel, M.B., Crasquin, S., Kershaw, S., and Collin, P.Y., 2013, In the aftermath of the

548   end-Permian extinction: the microbialite refuge?: Terra Nova, v. 25, no. 2, p. 137–

549   143, doi: 10.1111/ter.12017.

550   Forel, M.B., Crasquin, S., Kershaw, S., Feng, Q., and Collin, P.Y., 2009, Ostracods

551   (Crustacea) and water oxygenation in the earliest Triassic of South China:

552   implications for oceanic events at the end-Permian mass extinction: Australian

553   Journal of Earth Sciences, v. 56, no. 6, p. 815–823,

554   doi:10.1080/08120090903002631.

555 Forel, M.B., and Crasquin, S. 2015. Comment on the Chu et al., paper "Lilliput effect

556   in freshwater ostracods during the Permian-Triassic extinction"[Palaeogeography,

557   Palaeoclimatology, Palaeoecology v. 435, p. 38–52]: Palaeogeography,

558   Palaeoclimatology, Palaeoecology, v. 440, p. 860–862,

559   doi:10.1016/j.palaeo.2015.07.051.

560 Foster, W.J., Danise, S., Price, G.D., and Twitchett, R.J., 2017, Subsequent biotic crises

561   delayed marine recovery following the late Permian mass extinction event in

562   northern Italy: PLoS One, v. 12, no. 3, p. e0172321,

563   doi:10.1371/journal.pone.0172321.

564 Foster, W.J., Danise, S., and Twitchett, R.J., 2016, A silicified Early Triassic marine

565   assemblage from Svalbard: Journal of Systematic Palaeontology, v. 15, no. 10, p.

566   851–877, doi: 10.1080/14772019.2016.1245680.

567 Fraiser, M. L., and Bottjer, D. J., 2007, Elevated atmospheric CO_2 and the delayed biotic

568   recovery from the end-Permian mass extinction: Palaeogeography,

569   Palaeoclimatology, Palaeoecology, v. 252, no. 1–2, p. 164–175,

570   doi:10.1016/j.palaeo.2006.11.041.

571 Galfetti, T., Bucher, H., Martini, R., Hochuli, P.A., Weissert, H., Crasquin-Soleau, S.,

572   Brayard, A., Goudemand, N., Brühwiler, T., and Guodun, K., 2008, Evolution of

573   Early Triassic outer platform paleoenvironments in the Nanpanjiang Basin (South

574   China) and their significance for the biotic recovery: Sedimentary Geology, v. 204,

575   no. 1–2, p. 36–60, doi:10.1016/j.sedgeo.2007.12.008.

576 Godbold, A., Schoepfer, S., Shen, S., and Henderson, C.M., 2017, Precarious

577   ephemeral refugia during the earliest Triassic: Geology, p. G38793-1, doi:

578   10.1130/G38793.1.

579   Grasby, S.E., Beauchamp, B., Embry, A., and Sanei, H., 2013, Recurrent Early Triassic

580   ocean anoxia: Geology, v. 41, no. 2, p. 175–178, doi:10.1130/G33599.1.

581   Grasby, S.E., Beauchamp, B., and Knies, J., 2016, Early Triassic productivity crises

582   delayed recovery from world's worst mass extinction: Geology, v. 44, no. 9, p.

583   779–782, doi:10.1130/G38141.1.

584   Gu, Z.W., Huang, B.Y., Chen, C.Z. and others, 1976, Fossil Lamellibranchiata of China:

585   Science Press, Beijing, p. 1–512 (in Chinese).

586   Haig, D. W., Martin, S. K., Mory, A. J., McLoughlin, S., Backhouse, J., Berrell, R. W.,

587   Kear, B. P., Hall, R., Foster, C. B., Shi, G. R., and Bevan, J. C., 2015, Early Triassic

588   (early Olenekian) life in the interior of East Gondwana: mixed marine–terrestrial

589   biota   from   the   Kockatea   Shale,   Western   Australia: Palaeogeography,

590   palaeoclimatology,   palaeoecology, v.   417,   p.   511-533,

591   doi:10.1016/j.palaeo.2014.10.01.

592   Hallam, A., 1991, Why was there a delayed radiation after the end-Palaeozoic crisis?

593   Historical Biology, v. 5, no. 2–4, p. 257–262, doi:10.1080/10292389109380405.

594   Hauer, F. von, 1850, Ueber die von Herrn Bergrath W. Fuchs in den Venetianer Alpen

595   gesammelten Fossilien: Denkschriften der Akademie der Wissenschaften,

596   Mathematisch-Naturwissenschaftliche Klasse, v. 2, p. 109–126.

597   Hautmann, M., Bagherpour, B., Brosse, M., Frisk, Å., Hofmann, R., Baud, A., Nützel,

598   A., Goudemand, N., Bucher, H., and Brayard, A., 2015, Competition in slow

599   motion: the unusual case of benthic marine communities in the wake of the end-

600   Permian   mass   extinction: Palaeontology,   v.   58,   no.   5,   p.   871–901,

601   doi:10.1111/pala.12186.

602   Hautmann, M., Bucher, H., Brühwiler, T., Goudemand, N., Kaim, A., and Nützel, A.,

603   2011, An unusually diverse mollusc fauna from the earliest Triassic of South China

604   and its implications for benthic recovery after the end-Permian biotic crisis:

605   Geobios, v. 44, no. 1, p. 71–85, doi:10.1016/j.geobios.2010.07.004.

606   Hautmann, M., Smith, A.B., McGowan, A.J., and Bucher, H., 2013, Bivalves from the

607   Olenekian (Early Triassic) of south-western Utah: systematics and evolutionary

608   significance: Journal of Systematic Palaeontology, v. 11, no. 3, p. 263–293.

609   He, W.H., Shi, G.R., Twitchett, R.J., Zhang, Y., Zhang, K.X., Song, H.J., Yue, M.L.,

610   Wu, S.B., Wu, H.T., Yang, T.L., and Xiao, Y.F., 2015, Late Permian marine

611   ecosystem collapse began in deeper waters: evidence from brachiopod diversity

612   and body size changes: Geobiology, v. 13, p. 123–138, doi:10.1111/gbi.12119.

613   Hermann, E., Hochuli, P. A., Méhay, S., Bucher, H., Brühwiler, T., Ware, D., Hautmann,

614   M., Roohi, G., ur-Rehman, K., and Yaseen, A., 2011, Organic matter and

615   palaeoenvironmental signals during the Early Triassic biotic recovery: The Salt

616   Range and Surghar Range records: Sedimentary Geology, v. 234, no. 1–4, p. 19–

617   41, doi:10.1016/j.sedgeo.2010.11.003.

618   Hofmann, R., Goudemand, N., Wasmer, M., Bucher, H., and Hautmann, M., 2011, New

619   trace fossil evidence for an early recovery signal in the aftermath of the end-

620   Permian mass extinction: Palaeogeography, Palaeoclimatology, Palaeoecology, v.

621   310, no. 3-4, p. 216-226, doi:10.1016/j.palaeo.2011.07.014.

622   Hofmann, R., Hautmann, M., Brayard, A., Nützel, A., Bylund, K.G., Jenks, J.F., Vennin,

E., Olivier, N., Bucher, H., and Sevastopulo, G., 2014, Recovery of benthic marine communities from the end-Permian mass extinction at the low latitudes of eastern Panthalassa: Palaeontology, v. 57, no. 3, p. 547–589, doi: 10.1111/pala.12076.

Hofmann, R., Hautmann, M., and Bucher, H., 2013, A new paleoecological look at the Dinwoody Formation (Lower Triassic, western USA): intrinsic versus extrinsic controls on ecosystem recovery after the end-Permian mass extinction: Journal of Paleontology, v. 87, no. 05, p. 854–880, doi: 10.1666/12-153.

Hofmann, R., Hautmann, M., and Bucher, H., 2015, Recovery dynamics of benthic marine communities from the Lower Triassic Werfen Formation, northern Italy: Lethaia, v. 48, no. 4, p. 474–496, doi:10.1111/let.12121.

Huang, Y., Chen, Z.Q., Wignall, P.B., and Zhao, L., 2017, Latest Permian to Middle Triassic redox condition variations in ramp settings, South China: Pyrite framboid evidence: Geological Society of America Bulletin, v. 129, no. 1–2, p. 229–243, doi:10.1130/B31458.1.

Jiang, H., Lai, X., Sun, Y., Wignall, P.B., Liu, J., and Yan, C., 2014, Permian-Triassic conodonts from Dajiang (Guizhou, South China) and their implication for the age of microbialite deposition in the aftermath of the End-Permian mass extinction: Journal of Earth Science, v. 25, no. 3, p. 413–430, doi: 10.1007/s12583-014-0444-4.

Kaim, A., Nützel, A., Bucher, H., Brühwiler, T., and Goudemand, N., 2010, Early Triassic (Late Griesbachian) gastropods from South China (Shanggan, Guangxi): Swiss Journal of Geosciences, v. 103, no. 1, p. 121–128, doi:10.1007/s00015-

645   010-0005-5.

646   Kaim, A., Nützel, A., Hautmann, M., and Bucher, H., 2013, Early Triassic gastropods

647   from Salt Range, Pakistan: Bulletin of Geosciences, p. 505–516, doi:

648   10.3140/bull.geosci.1395.

649   Krystyn, L., Richoz, S., Baud, A., and Twitchett, R.J., 2003, A unique Permian–Triassic

650   boundary section from the Neotethyan Hawasina Basin, Central Oman Mountains:

651   Palaeogeography, Palaeoclimatology, Palaeoecology, v. 191, no. 3–4, p. 329–344,

652   doi:10.1016/S0031-0182(02)00670-3.

653   Lau, K. V., Maher, K., Altiner, D., Kelley, B. M., Kump, L. R., Lehrmann, D. J., Silva-

654   Tamayo, J. C., Weaver, K. L., Yu, M. Y., and Payne, J. L., 2016, Marine anoxia

655   and delayed Earth system recovery after the end-Permian extinction: Proceedings

656   of the National Academy of Sciences, v. 113, no. 9, p. 2360–2365.

657   doi.10.1073/pnas.1515080113.

658   Lehrmann, D. J., 1999, Early Triassic calcimicrobial mounds and biostromes of the

659   Nanpanjiang basin, south China: Geology, v. 27, no. 4, p. 359-362.

660   Leonardi, P., 1935, 2.Trias inferiore delle Venezie: Memoirie degli Istituti de Geologia

661   e Mineralogia dell'Università di Padova v. 11, p. 1–136.

662   Li, G., Wang, Y., Shi, G. R., Liao, W., and Yu, L., 2016, Fluctuations of redox conditions

663   across the Permian–Triassic boundary—New evidence from the GSSP section in

664   Meishan of South China: Palaeogeography, Palaeoclimatology, Palaeoecology, v.

665   448, p. 48-58, doi:10.1016/j.palaeo.2015.09.050.

666   Liao, W., Bond, D. P., Wang, Y., He, L., Yang, H., Weng, Z., and Li, G., 2017, An

667   extensive anoxic event in the Triassic of the South China Block: A pyrite framboid

668   study from Dajiang and its implications for the cause (s) of oxygen

669   depletion: Palaeogeography, Palaeoclimatology, Palaeoecology, v. 486, p. 86-95,

670   doi:10.1016/j.palaeo.2016.11.012.

671   Liu, L., 1964, Early Triassic bivalves from eastern Qinling, Shaanxi province: Acta

672   Palaeontologica Sinica, v. 12, no. 2, p. 312–322 (in Chinese).

673   Liu, L., Wu, Y.S., Li, Y., Liu, Q.S., Jiang, H.X., and Liu, H., 2017, Microfacies of a

674   Permian calcisponge reef in Lichuan, western Hubei, South China: Palaeoworld,

675   doi: 10.1016/j.palwor.2017.05.006.

676   Meyer, K. M., Yu, M., Jost, A. B., Kelley, B. M., and Payne, J. L., 2011, $\delta^{13}C$ evidence

677   that high primary productivity delayed recovery from end-Permian mass

678   extinction: Earth and Planetary Science Letters, v. 302, no. 3–4, p. 378–384, doi:

679   10.1016/j.epsl.2010.12.033.

680   Miklukho-Maklay, K.V., 1954, Foraminifers of the Upper Permian Deposits of the

681   Northern Caucasus: Trudy Vsesoyuznogo NauchnoIssledovatel'skogo

682   Geologicheskogo Instituta (VSEGEI). Ministerstva Geologii i Okhrani Nedr, p. 1-

683   163.

684   Motani, R., Jiang, D. Y., Chen, G. B., Tintori, A., Rieppel, O., Ji, C., and Huang, J. D.,

685   2015, A basal ichthyosauriform with a short snout from the Lower Triassic of

686   China: Nature, v. 517, no. 7535, p. 485–488, doi:10.1038/nature13866.

687   Mu, L., Zakharov, Y., Li, W. and Shen, S., 2007, Early Induan (Early Triassic)

688   cephalopods from the Daye Formation at Guiding, Guizhou Province, South

689   China: Journal of Paleontology, v. 81, no. 5, p. 858–872, doi: 0022-

690   3360/07/0081-858$03.00.

691   Nützel, A., 2005, Recovery of gastropods in the Early Triassic: Comptes Rendus

692   Palevol, v. 4, no. 6–7, p. 501–515, doi:10.1016/j.crpv.2005.02.007.

693   Orchard, M.J., 2007, Conodont diversity and evolution through the latest Permian and

694   Early Triassic upheavals: Palaeogeography, Palaeoclimatology, Palaeoecology, v.

695   252, no. 1–2, p. 93–117, doi:10.1016/j.palaeo.2006.11.037.

696   Patte, E., 1935, Fossils paleozoiques et mesodu Sud-Ouest de la Chine: Palaeontologia

697   Sinica Series B, v. 15, p. 1–50.

698   Payne, J.L., 2005, Evolutionary dynamics of gastropod size across the end-Permian

699   extinction and through the Triassic recovery interval, Paleobiology, Volume 31, p.

700   269–290.

701   Payne, J.L., Lehrmann, D.J., Wei, J., and Knoll, A.H., 2006, The Pattern and Timing of

702   Biotic Recovery from the End-Permian Extinction on the Great Bank of Guizhou,

703   Guizhou   Province,   China: Palaios,   v.   21,   no.   1,   p.   63–85,

704   doi:10.2110/palo.2005.p05-12p.

705   Payne, J.L., Summers, M., Rego, B.L., Altiner, D., Wei, J., Yu, M., and Lehrmann, D.

706   J., 2011, Early and Middle Triassic trends in diversity, evenness, and size of

707   foraminifers on a carbonate platform in south China: implications for tempo and

708   mode of biotic recovery from the end-Permian mass extinction: Paleobiology, v.

709   37, no. 3, p. 409–425, doi: 10.1666/08082.1.

710   Payne, J.L., Turchyn, A.V., Paytan, A., DePaolo, D.J., Lehrmann, D.J., Yu, M., and Wei,

711   J., 2010, Calcium isotope constraints on the end-Permian mass extinction:

712   Proceedings of the National Academy of Sciences, v. 107, no. 19, p. 8543–8548,

713   doi: 10.1073/pnas.0914065107.

714   Pietsch, C., and Bottjer, D.J., 2014, The importance of oxygen for the disparate

715   recovery patterns of the benthic macrofauna in the Early Triassic: Earth-Science

716   Reviews, v. 137, p. 65–84, doi:10.1016/j.earscirev.2013.12.002.

717   Raup, D.M., 1979, Size of the Permo-Triassic bottleneck and its evolutionary

718   implications: Science, v. 206, p. 217–218.

719   Romano, C., Goudemand, N., Vennemann, T.W., Ware, D., Schneebeli-Hermann, E.,

720   Hochuli, P.A., Brühwiler, T., Brinkmann, W., and Bucher, H., 2013, Climatic and

721   biotic upheavals following the end-Permian mass extinction: Nature Geoscience,

722   v. 6, no. 1, p. 57–60, doi:10.1038/ngeo1667.

723   Sepkoski Jr, J.J., 1981, A factor analytic description of the Phanerozoic marine fossil

724   record: Paleobiology, v. 7, no. 1, p. 36–53, doi:10.1017/S0094837300003778.

725   Shigeta, Y., Zakharov, Y.D., Maeda, H., and Popov, A.M., 2009, The Lower Triassic

726   System in the Abrek Bay Area, South Primorye, Russia: Tokyo: National Museum

727   of Nature and Science, p. 1–218.

728   Scheyer, T.M., Romano, C., Jenks, J., and Bucher, H., 2014, Early Triassic marine biotic

729   recovery: the predators' perspective. Plos One, v. 9, no. 3, p. e88987,

730   doi:10.1371/journal.pone.0088987.

731   Scotese, C.R. 2001. Atlas of earth history. University of Texas at Arlington.

732   Department of Geology. PALEOMAP Project.

733   Song, H., Jiang, G., Poulton, S. W., Wignall, P. B., Tong, J., Song, H., An, Z., Chu, D.,

734   Tian, L., She, Z., and Wang, C., 2017, The onset of widespread marine red beds

735   and the evolution of ferruginous oceans: Nature Communications, v. 8, no. 1, p.

736   399, doi:10.1038/s41467-017-00502-x.

737   Song, H., Tong, J., and Chen, Z.Q., 2011, Evolutionary dynamics of the Permian–

738   Triassic foraminifer size: evidence for Lilliput effect in the end-Permian mass

739   extinction and its aftermath: Palaeogeography, Palaeoclimatology,

740   Palaeoecology, v. 308, no. 1, p. 98–110, doi:10.1016/j.palaeo.2010.10.036.

741   Song, H., Wignall, P.B., Chen, Z.Q., Tong, J., Bond, D.P.G., Lai, X., Zhao, X., Jiang,

742   H., Yan, C., Niu, Z., Chen, J., Yang, H., and Wang, Y., 2011, Recovery tempo and

743   pattern of marine ecosystems after the end-Permian mass extinction: Geology, v.

744   39, no. 8, p. 739–742, doi:10.1130/G32191.1.

745   Song, H., Wignall, P.B., Chu, D., Tong, J., Sun, Y., Song, H., He, W., and Tian, L.,

746   2014, Anoxia/high temperature double whammy during the Permian-Triassic

747   marine crisis and its aftermath: Scientific Reports, v. 4, p. 1–7,

748   doi:10.1038/srep04132.

749   Song, H., Wignall, P.B., Tong, J., Bond, D.P., Song, H., Lai, X., Zhang, K., Wang, H.

750   and Chen, Y. 2012. Geochemical evidence from bio-apatite for multiple oceanic

751   anoxic events during Permian-Triassic transition and the link with end-Permian

752   extinction and recovery: Earth and Planetary Science Letters, v. 353, no. 2012, p.

753   12–21, doi.org/10.1016/j.epsl.2012.07.005.

754   Song, H., Wignall, P.B., Tong, J., and Yin, H. 2013. Two pulses of extinction during

755   the Permian-Triassic crisis: Nature Geoscience, v. 6, no. 1, p. 52–56,

756   doi:10.1038/NGEO1649.

757   Stanley, S.M., 2009, Evidence from ammonoids and conodonts for multiple Early

758   Triassic mass extinctions: Proceedings of the National Academy of Sciences, v.

759   106, no. 36, p. 15264–15267, doi:10.1073/pnas.0907992106.

760   Stanley, S.M. 2016, Estimates of the magnitudes of major marine mass extinctions in

761   earth history: Proceedings of the National Academy of Sciences, v. 113, no. 42, p.

762   E6325–E6334, doi:10.1073/pnas.1613094113.

763   Sun, Y., Joachimski, M.M., Wignall, P.B., Yan, C., Chen, Y., Jiang, H., Wang, L., and

764   Lai, X., 2012, Lethally Hot Temperatures During the Early Triassic Greenhouse:

765   Science, v. 338, no. 6105, p. 366–370, doi:10.1126/science.1224126.

766   Tian, L., Tong, J., Algeo, T.J., Song, H., Song, H., Chu, D., Shi, L., and Bottjer, D.J.

767   2014. Reconstruction of Early Triassic ocean redox conditions based on

768   framboidal pyrite from the Nanpanjiang Basin, South China: Palaeogeography,

769   Palaeoclimatology,   Palaeoecology,   v.   412,   p.   68–79,

770   doi.org/10.1016/j.palaeo.2014.07.018.

771   Tong, J., Zuo, J., and Chen, Z.Q., 2007, Early Triassic carbon isotope excursions from

772   South China: Proxies for devastation and restoration of marine ecosystems

773   following the end-Permian mass extinction: Geological Journal, v. 42, p. 371–389,

774   doi:10.1002/gj.1084.

775   Twitchett, R.J., 2007, The Lilliput effect in the aftermath of the end-Permian extinction

776   event: Palaeogeography, Palaeoclimatology, Palaeoecology, v. 252, p. 132–144,

777   doi:10.1016/j.palaeo.2006.11.038.

778   Twitchett, R.J., Krystyn, L., Baud, A., Wheeley, J.R., and Richoz, S., 2004, Rapid

779   marine recovery after the end-Permian mass-extinction event in the absence of

780   marine anoxia: Geology, v. 32, no. 9, p. 805–808, doi:10.1130/G20585.1.

781   Wang, F., Chen, J., Dai, X., and Song, H., 2017, A new Dienerian (Early Triassic)

782   brachiopod fauna from South China and implications for biotic recovery after the

783   Permian-Triassic extinction: Papers in Palaeontology, v. 3, no. 3, p. 425–439, doi:

784   10.1002/spp2.1083.

785 Ware, D., Bucher, H., Brayard, A., Schneebeli-Hermann, E., and Brühwiler, T., 2015,

786   High-resolution biochronology and diversity dynamics of the Early Triassic

787   ammonoid recovery: The Dienerian faunas of the Northern Indian Margin:

788   Palaeogeography, Palaeoclimatology, Palaeoecology, v. 440, p. 363–373,

789   doi:10.1016/j.palaeo.2015.09.013.

790 Wasmer, M., Hautmann, M., Hermann, E., Ware, D., Roohi, G., Ur-Rehman, K., Yaseen,

791   A., and Bucher, H., 2012, Olenekian (Early Triassic) bivalves from the Salt Range

792   and Surghar Range, Pakistan: Palaeontology, v. 55, no. 5, p. 1043–1073,

793   doi:10.1111/j.1475-4983.2012.01176.x.

794 Wignall, P.B., Bond, D.P.G., Sun, Y.D., Grasby, S.E., Beauchamp, B., Joachimski,

795   M.M., and Blomeier, D.P.G., 2016, Ultra-shallow marine anoxia in an Early

796   Triassic shallow-marine clastic ramp (Spitsbergen) and the suppression of benthic

797   radiation: Geological Magazine, v. 153, p. 316–331,

798   doi:10.1017/S0016756815000588.

799 Wignall, P. B., and Twitchett, R. J., 1996, Oceanic anoxia and the end-Permian mass

800   extinction: Science, v. 272, no. 5265, p. 1155–1158.

801 Xiao, Y., Suzuki, N., and He, W., 2017, Water depths of the latest Permian

802   (Changhsingian) radiolarians estimated from correspondence analysis: Earth-

803   Science Reviews, v. 173, p. 141–158, doi:10.1016/j.earscirev.2017.08.012.

804 Xu, G., 1988, Early Triassic cephalopods from Lichuan, Western Hubei: Acta

805   Palaeontologica Sinica, v. 27, no. 4, p. 437–456, (in Chinese, with English

806   summary).

807   Yang, H., Chen, Z.Q., Wang, Y., Tong, J., Song, H., and Chen, J., 2011, Composition

808   and structure of microbialite ecosystems following the end-Permian mass

809   extinction in South China: Palaeogeography, Palaeoclimatology, Palaeoecology, v.

810   308, no. 1–2, p. 111–128, doi:10.1016/j.palaeo.2010.05.029.

811   Yin, H., Jiang, H., Xia, W., Feng, Q., Zhang, N., and Shen, J., 2014, The end-Permian

812   regression in South China and its implication on mass extinction: Earth-Science

813   Reviews, v. 137, p. 19–33, doi: 10.1016/j.earscirev.2013.06.003.

814   Zhang, K., Tong, J., Shi, G. R., Lai, X., Yu, J., He, W., Peng, Y., and Jin, Y., 2007, Early

815   Triassic conodont–palynological biostratigraphy of the Meishan D Section in

816   Changxing, Zhejiang Province, South China: Palaeogeography,

817   Palaeoclimatology, Palaeoecology, v. 252, no. 1–2, p. 4–23,

818   doi:10.1016/j.palaeo.2006.11.031.

819   Zheng, Z., 1981, Uppermost Permian (Changhsingian) ammonoids from Western

820   Guizhou: Acta Palaeontologica Sinica, v. 20, no. 2, p. 107–114, (in Chinese, with

821   English abstract).

822

823   **FIGURE CAPTIONS**

824
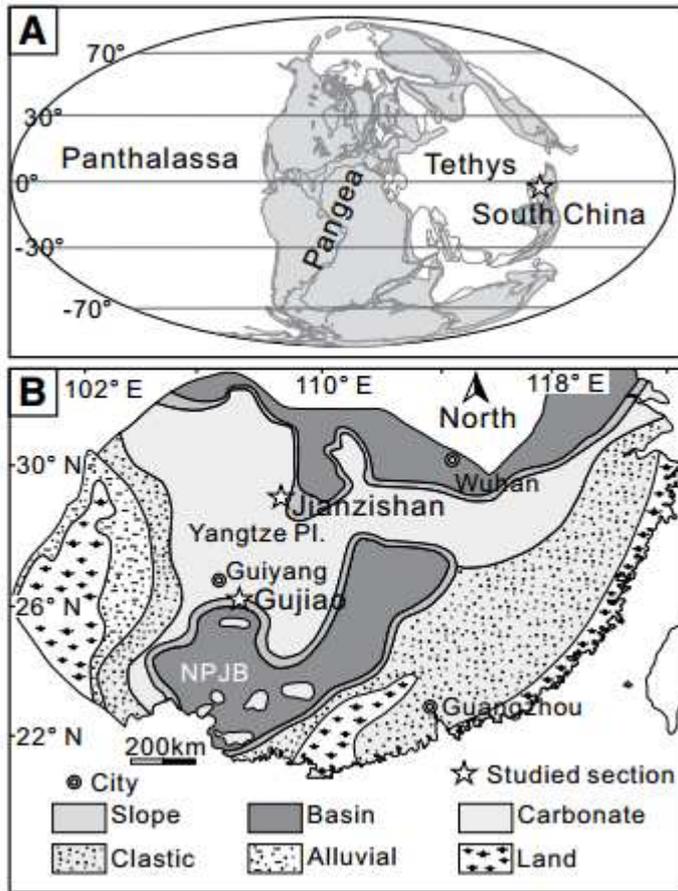
Figure 1. A. Early Triassic paleogeography, modified from Scotese (2001). B. Early

Triassic paleogeographic map of South China, modified from Feng et al. (1997). PL.

platform; NPJB. Nanpanjiang Basin.
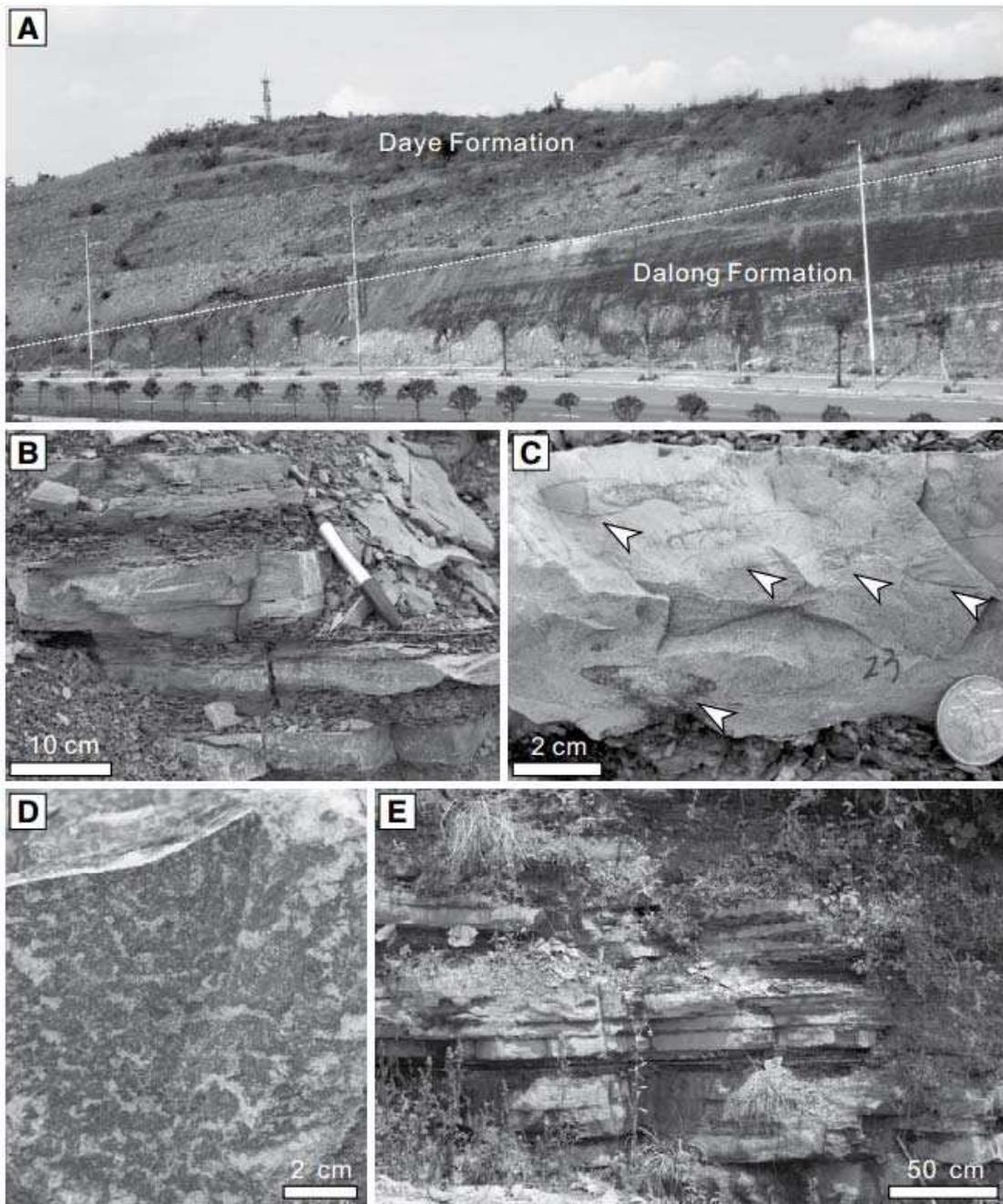
828

829 Figure 2. A. Landscape view of the Gujiao section. B. Laminated marlstones alternated

830 with black shales of the Daye Formation at Gujiao. C. Light gray marlstones with

831 abundant ammonoids (indicated by white arrows). D. Microbialites from the lower

832 most of the Daye Formation at Jianzishan. E. Mudstones alternating with shales

833 overlying the microbialites at Jianzishan.
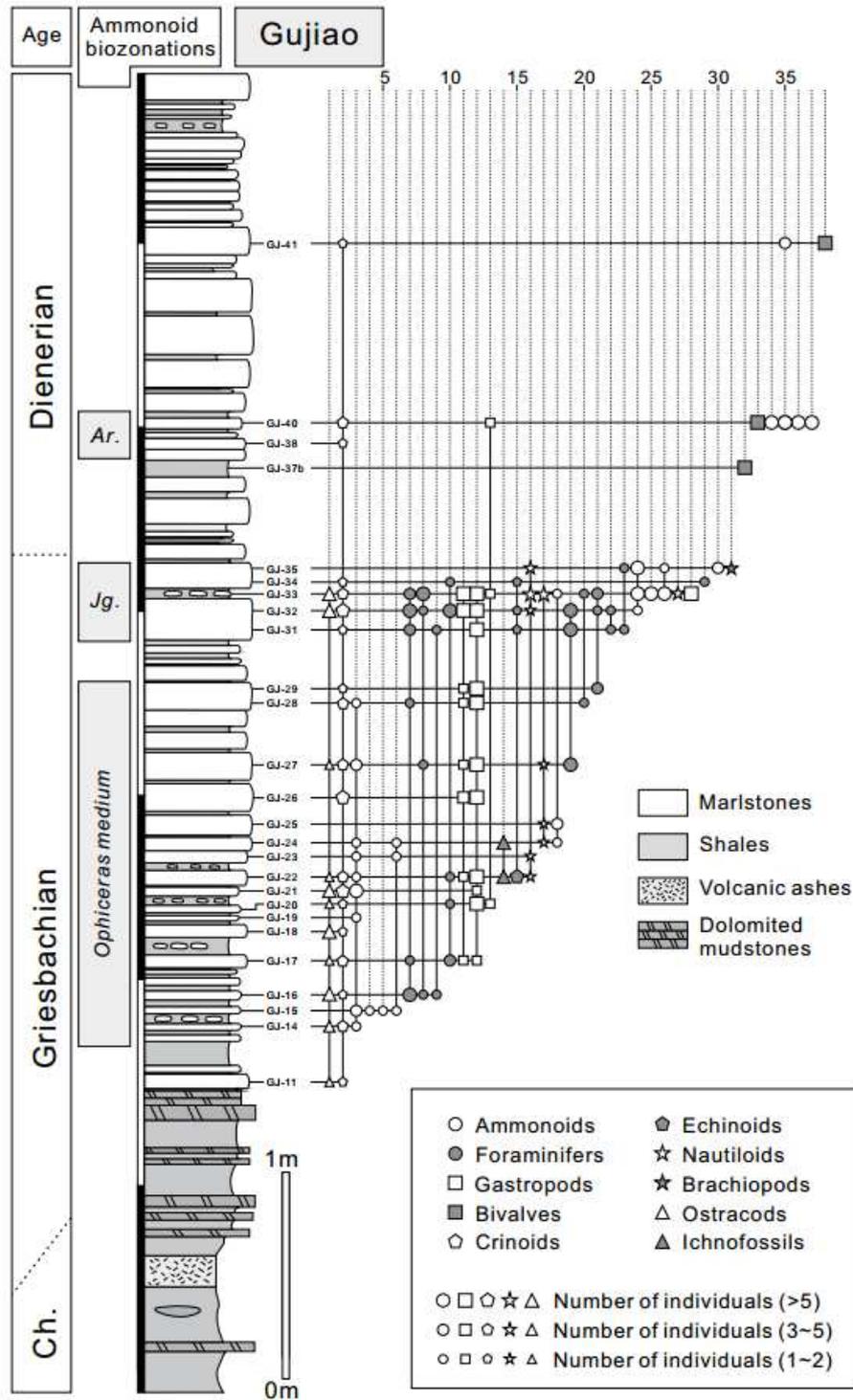
834

835 Figure 3. Fossil occurrences in the Gujiao section. See Table 1 for fossil list. Ch.

836 Changhsingian; *Ar*. *Ambites radiatus* bed; *Jg*. *Jieshaniceras guizhouense* beds.
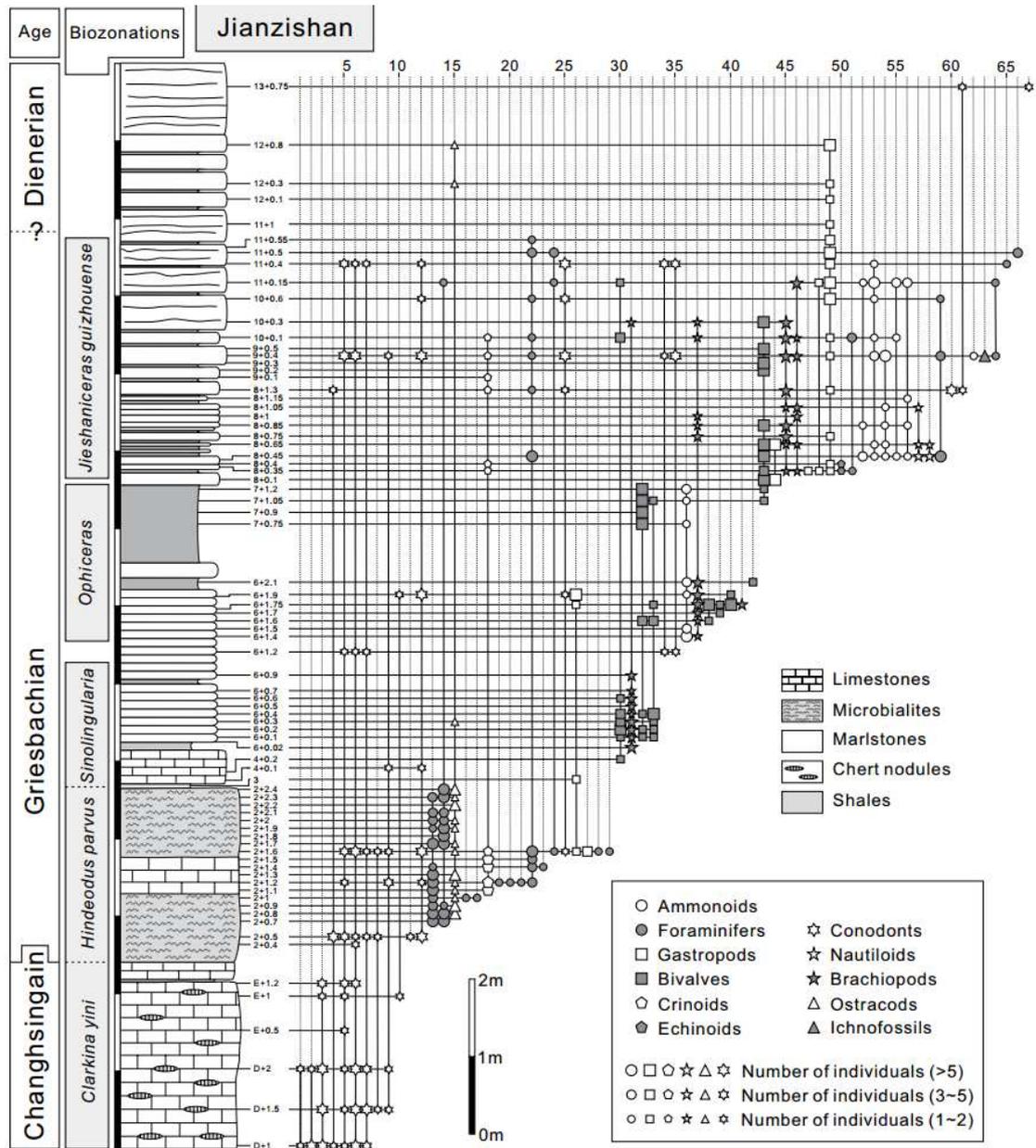
Figure 4. Fossil occurrences in the Jianzishan section. Conodont data and part of ammonoid data are from Bai et al. (2017). Brachiopod data are from Wang et al. (2017). See Table 2 for fossil list.

841
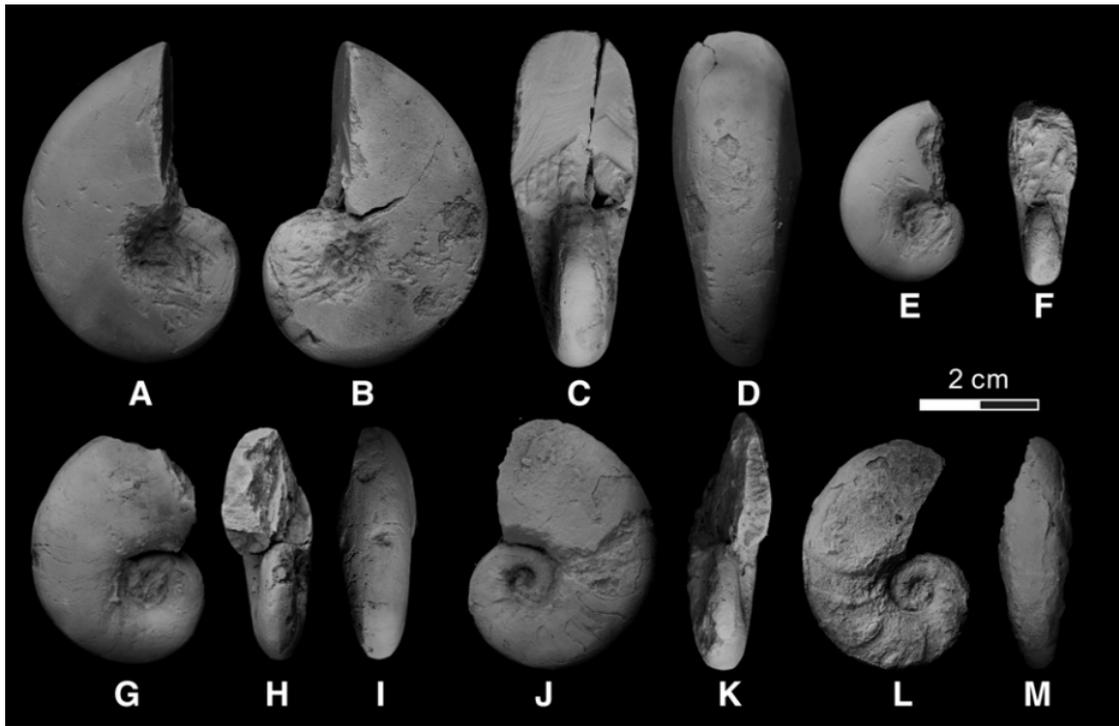
Figure 5. Nautiloids from bed GJ-33, Gujiao section. A-D. *Xiaohenautilus sinensis* Xu,

1988; E-F. *Xiaohenautilus sinensis* Xu, 1988; G-I. *Xiaohenautilus huananensis* Xu,

1988; J-K. *Xiaohenautilus huananensis* Xu, 1988; L M. undetermined nautiloid.

845
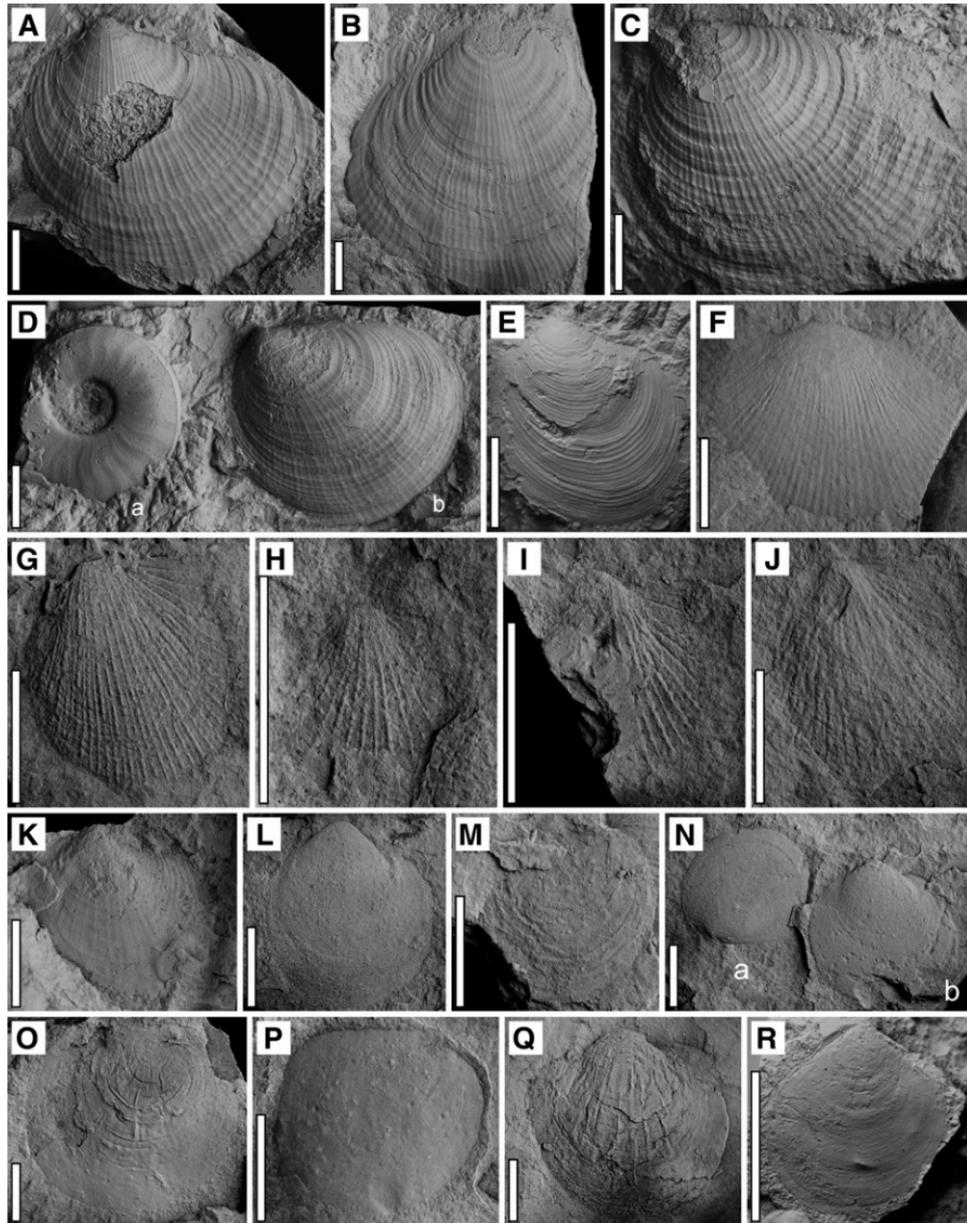
Figure 6. Mollusks from the Gujiao and Jianzishan sections. Scale bar is 1 cm. A-C.

Claraia radialis (Leonardi, 1935), A, left valve, from GJ-40, B, right valve, from GJ-

40, C, left valve, from GJ-40; D. a. *Ambites radiatus* (Brühwiler, Brayard, Bucher and

Kuang, 2008), b. *Claraia radialis* (Leonardi, 1935), left valve, from GJ-40; E. *Claraia*

aurita (von Hauer, 1850), left valve, from GJ-41; F. *Claraia stachei* (Patte, 1935), left

valve, from GJ-37b; G-J. *Eumorphotis venetiana* (von Hauer, 1850), G, left valve, from

JZS-6+0.3, H, left valve, from JZS-6+0.35, I, left valve, from JZS-6+0.3, J, left valve,

853 from JZS-6+0.3; K-N. *Claraia wangi* (Patte, 1935), K, left valve, from JZS-6+0.45, L,

854 left valve, from JZS- 7+0.75, M, left valve, from JZS-7+1.05, N, a. left valve, b. right

855 value, from JZS-7+1.2; O-Q. *Claraia zhenanica* Chen and Liu in Liu, 1964, O, right

856 valve, from JZS-8+0.65, P, right valve, from JZS-8+0.65, Q, left valve, from JZS-9+0.2;

857 R. *Scythentolium scutigerulus* Hautmann et al., 2011, left valve, From JZS-6+1.9.
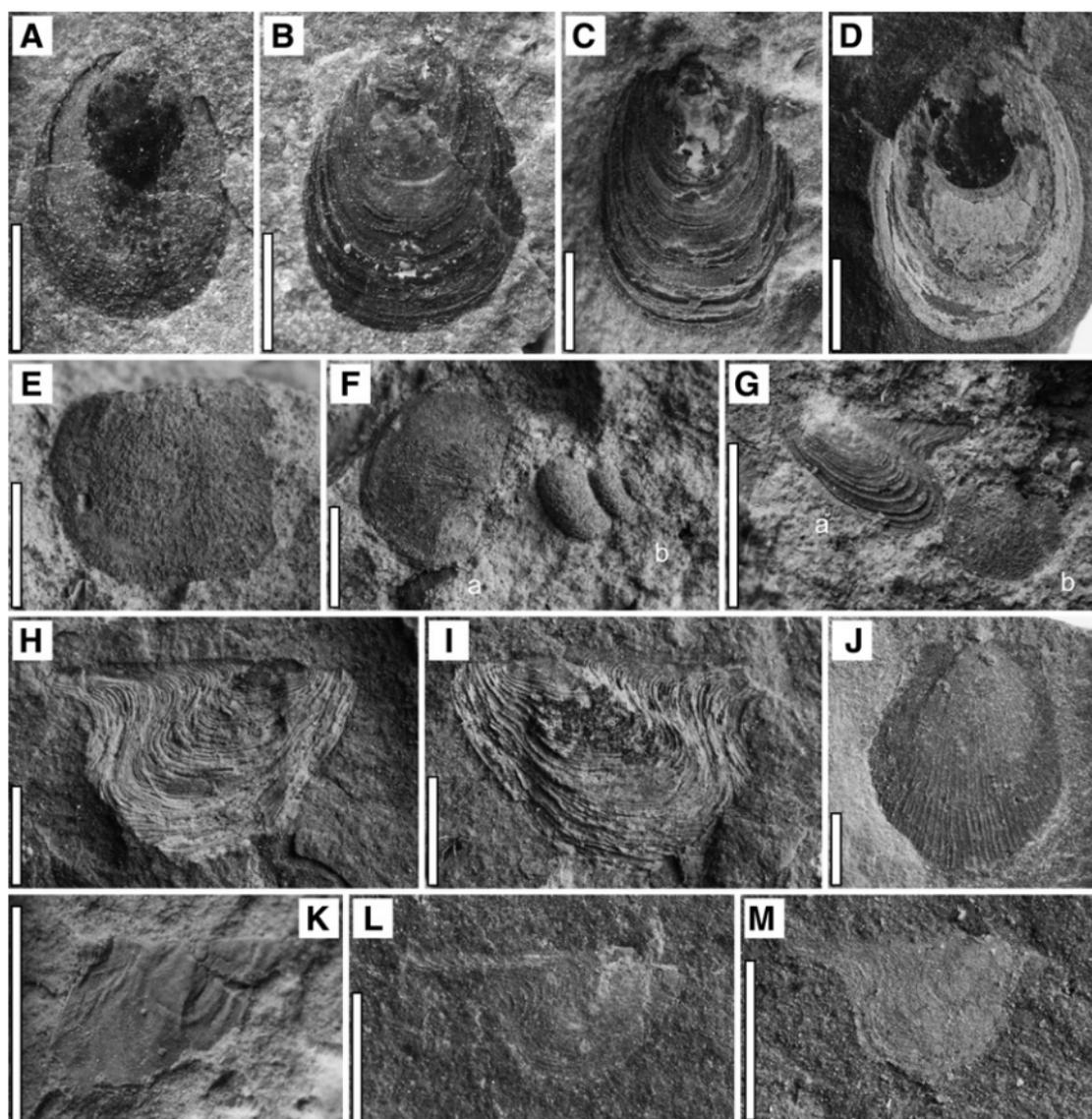
858

859 Figure 7. Brachiopods, bivalves and gastropods from the Jianzishan section. The scale

860 bar is 2 mm. A-D. *Sinolingularia* sp. indet.; A, from JZS-6+0.02; B, from JZS-6+0.3;

861 C, from JZS- 6+0.9; D, from JZS-10+0.3; E. *Crurithyris* sp. indet., from JZS-6+1.9; F.

862   a. *Crurithyris* sp. indet., b. ?*Pseudomurchisonia* sp. indet., from JZS-6+1.9; G. a. *Pteria*

863   *ussurica variabilis* Chen and Lan in Gu et al, 1976, left valve; b. *Crurithyris* sp. indet.,

864   from JZS-6+1.75; H. *Pteria ussurica variabilis* Chen and Lan in Gu et al, 1976, left

865   valve, external mold, from JZS-6+1.75; I. *Pteria ussurica variabilis* Chen and Lan in

866   Gu et al, 1976, left valve, from JZS-6+1.75; J. *Eumorphotis* sp. indet., left valve, from

867   JZS-6+1.75; K. *Eumorphotis* sp. indet., right valve, from JZS-6+1.7; L. *Pteria ussurica*

868   *variabilis* Chen and Lan in Gu et al, 1976, right valve, from JZS-6+1.75; M. *Pteria*

869   *ussurica variabilis* Chen and Lan in Gu et al, 1976, right valve, from JZS-6+1.75.

870
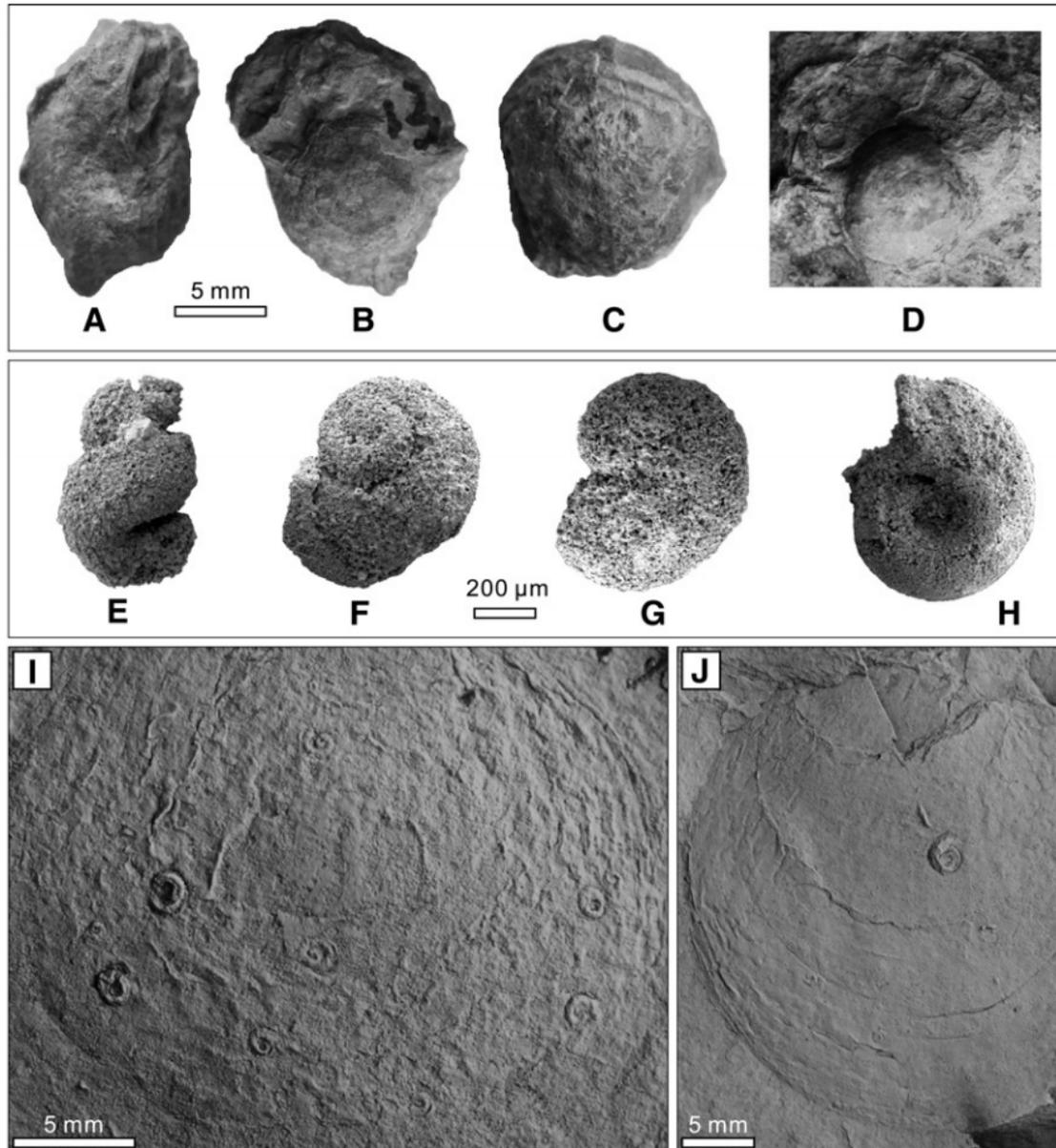
Figure 8. Gastropods and microconchids from the Gujiao and Jianzishan sections. A-D.
Bellerophontidae gen. indet., from bed GJ-33; E. undetermined Gastropod A., from bed
JZS-6+1.9; F-G. ?*Naticopsis* sp. indet., from bed JZS-6+1.9; H. Bellerophontidae gen.
indet., from bed JZS-6+1.9. I-J, epizoan microconchids on *Claraia* shells, from bed
JZS-8+0.65.
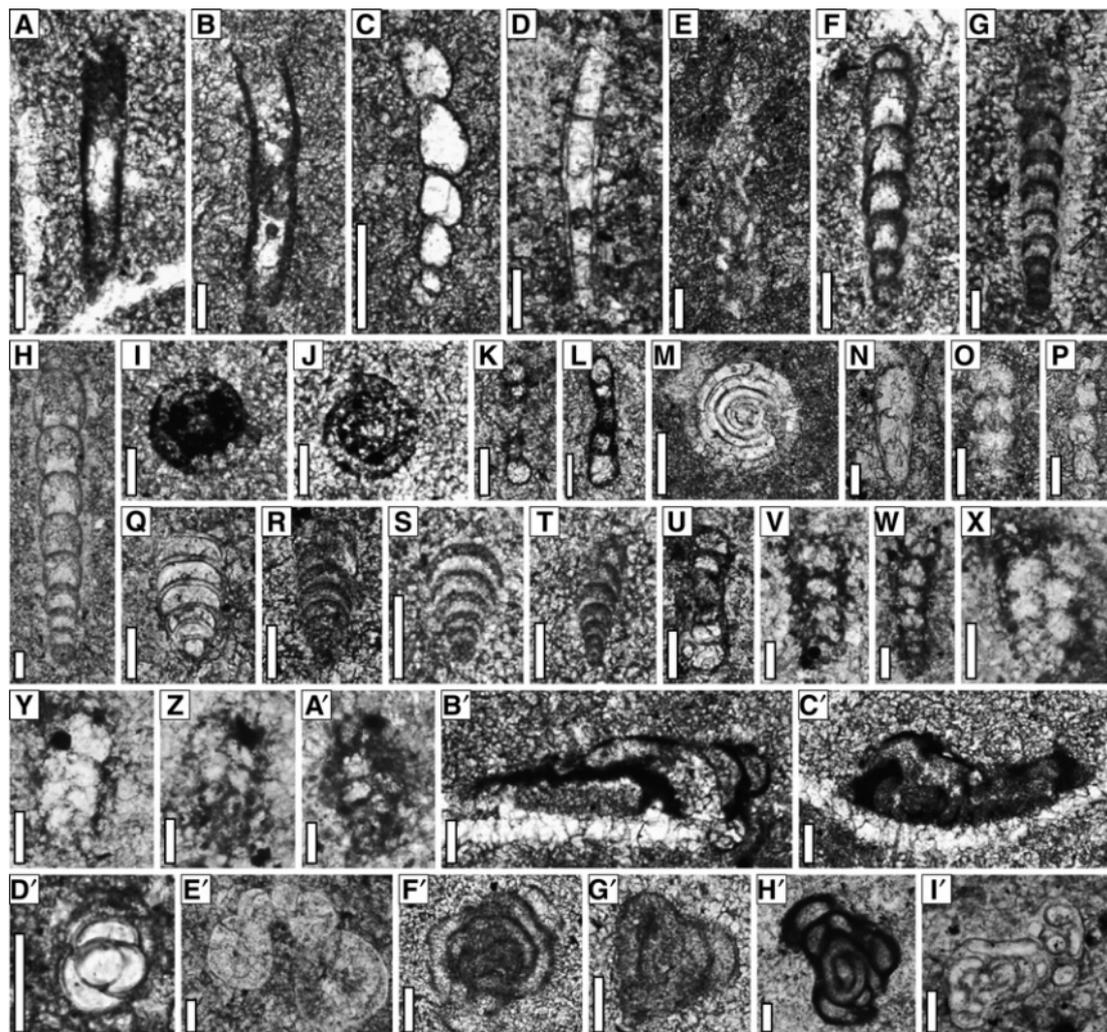
Figure 9. Foraminifers from the Gujiao and Jianzishan sections. The scale bar is 50 μm.

A-B. *Earlandia* sp. indet., from JZS-2+0.7; C. *Dentalina* sp. indet., from JZS-2+1; D.

Tezaquina sp. indet., from JZS-2+1.2; E. *Vervilleina* sp., indet., from JZS-11+0.4; F-H.

Nodosinelloides sagitta (Miklukho-Maklay, 1954), F-G, from JZS-11+0.5, H, from GJ-

28; I-L, *Postcladella kalhori* (Brönnimann, Zaninetti and Bozorgnia, 1972), I-J, from

JZS-2+0.7, K-L from JZS-2+2.3; M. *Ammodiscus* sp. indet., from JZS-2+1; N.

"*Nodosaria*" sp. indet., from JZS-2+1.2; O. "*Nodosaria*" *elabugae* Cherdyntsev, 1914,

from JZS-2+1.6; P. "*Nodosaria*" *skyphica* Efimova, 1974, from JZS-2+1.6; Q-S.

Geinitzina sp. indet., Q, from JZS-2+1.6, R-S, from JZS-11+0.4; T. *Frondina* sp. indet.,

886 from JZS-9+0.4; U. *Hemigordius* sp. indet., from JZS-2+1.2; V-W. ?*Dagmarita* sp.

887 indet., V, from GJ-29, W, from GJ-33; X-A'. *Gaudryina* sp. indet., X-Z, from GJ-32, A',

888 from GJ-33; B'-C'. *Tolypammina* sp. indet., from JZS-9+0.4; D'. ?*Duotaxis* sp. indet.,

889 from JZS-2+1.4; E'. *Duotaxis* sp. indet., from GJ-28; F'-I'. *Glomospira* sp. indet., F'-

890 G', from JZS-10+0.1, H' from JZS-8+0.35, I' from GJ-31.
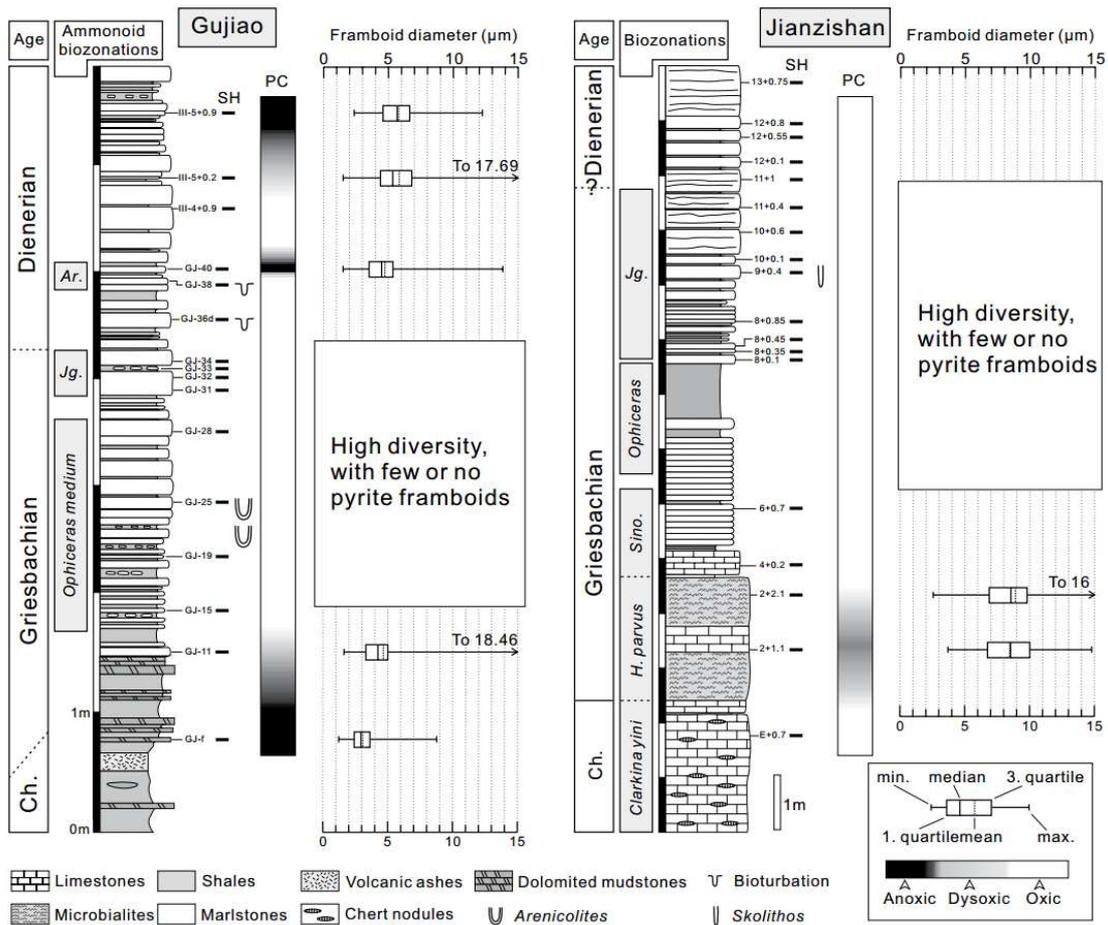
891

892 Figure 10. Griesbachian-Dienerian paleoredox conditions of the Gujiao and Jianzishan

893 sections. Only five samples yield pyrite framboids at Gujiao, and two at Jianzishan. SH:

894 pyrite sample horizon. PC: Paleoredox conditions. Biozonations abbreviation. *Jg.*

895 *Jieshaniceras guizhouense* beds; *Ar. Ambites radiatus* bed; *H. Hindeodus*; *Sino.*

896 *Sinolingularia* beds.
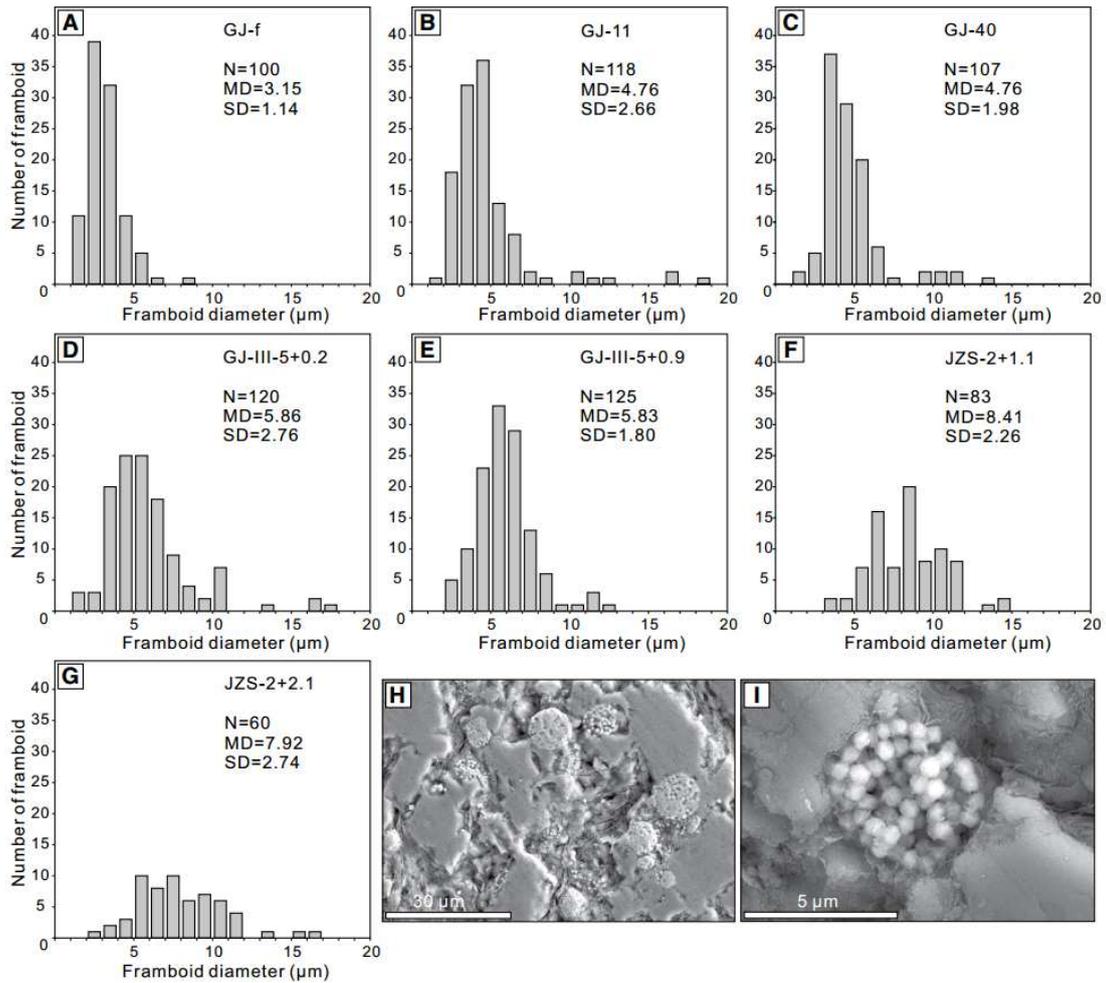
897

898   Figure 11. A-G. Size distributions of pyrite framboids. H-I. SEM photos of typical

899   pyrite framboids, from sample GJ-III- 5+0.9.
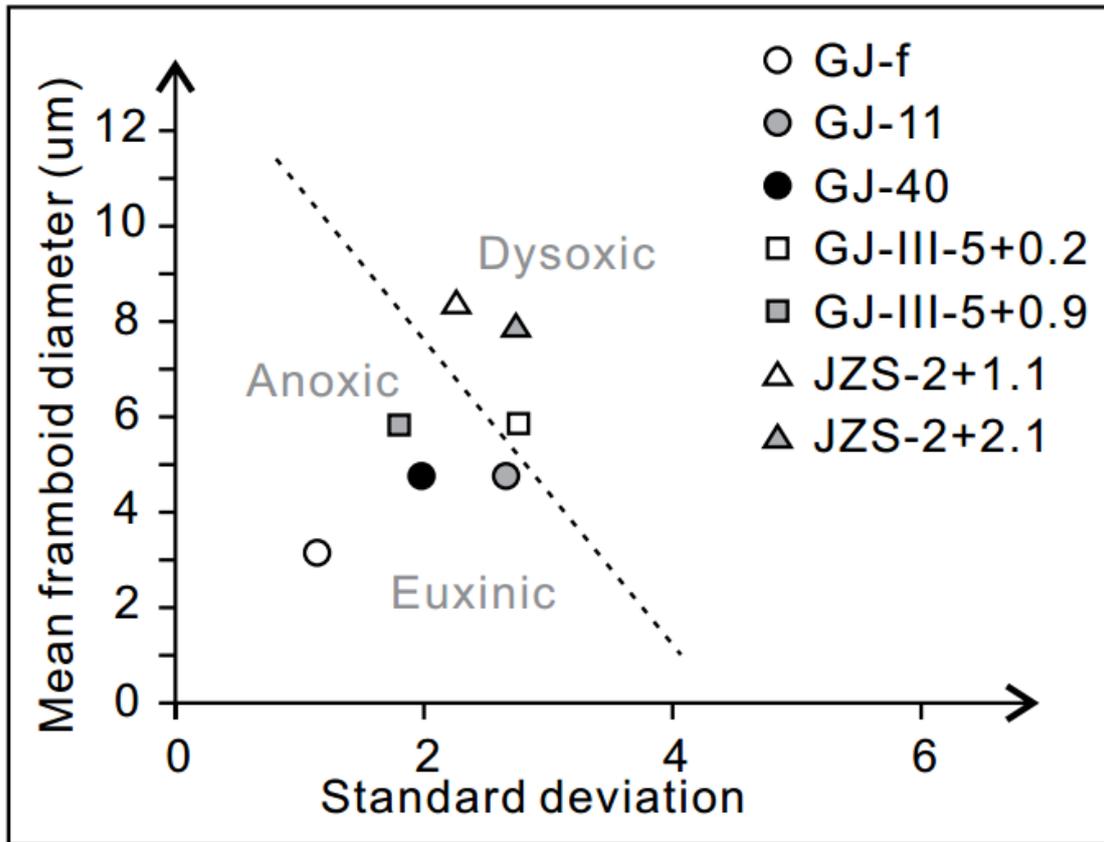
900

901 Figure 12. Mean diameter versus standard deviation of pyrite framboids. The dotted

902 line separating euxinic/anoxic from dysoxic facies is from Bond and Wignall (2010)

903 and Tian et al., (2014) and is derived from measurements in modern environments.
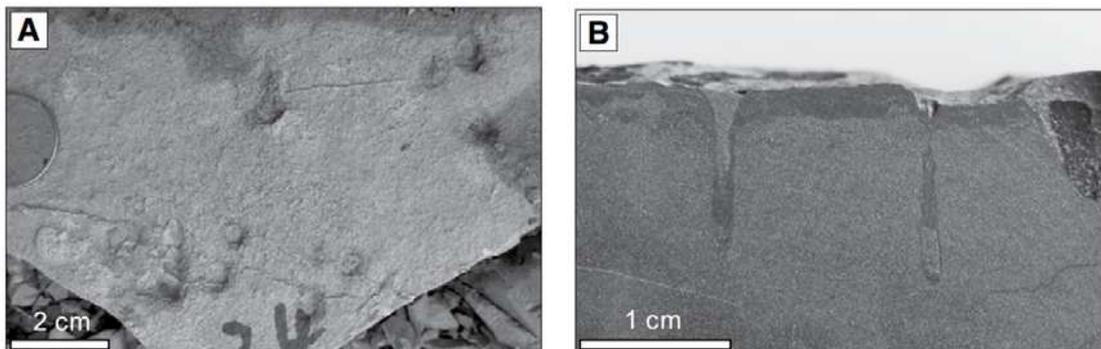
904

905 Figure 13. Ichnofossils from the Gujiao and Jianzishan sections. A, *Arenicolites* isp.,

906 from bed GJ-24. B, *Skolithos* isp., from bed JZS-9+0.4.
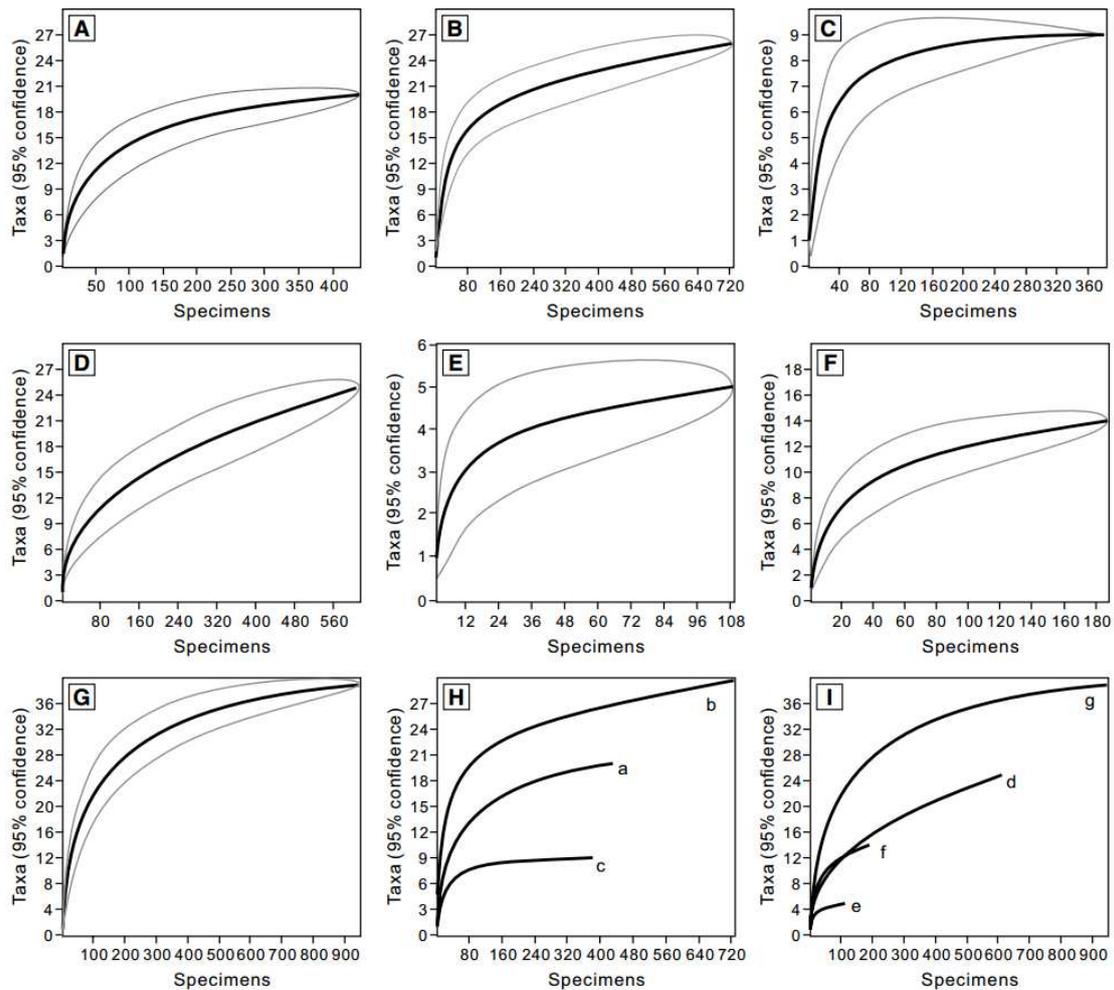
Figure 14. Rarefaction analyses for each analyzed zone or beds. The grey lines indicate 95% confidence intervals. The *Jieshaniceras guizhouense* beds in both sections contain the highest taxonomic richness. A, *Ophiceras medium* beds, Gujiao section. B, *Jieshaniceras guizhouense* beds, Gujiao section. C, *Ambites radiatus* bed, Gujiao section. D, *Hindeodus parvus* Zone, Jianzishan section. E, *Sinolingularia* beds, Jianzishan section. F, *Ophiceras medium* beds, Jianzishan section. G, *Jieshaniceras guizhouense* beds, Jianzishan section. H, rarefaction for each bed at Gujiao, a, *Ophiceras medium* beds; b, *Jieshaniceras guizhouense* beds; c, *Ambites radiatus* bed. I, rarefaction for each biozone/assemblage at Jianzishan, d, *Hindeodus parvus* Zone, e, *Sinolingularia* beds, f, *Ophiceras medium* beds, g, *Jieshaniceras guizhouense* beds.
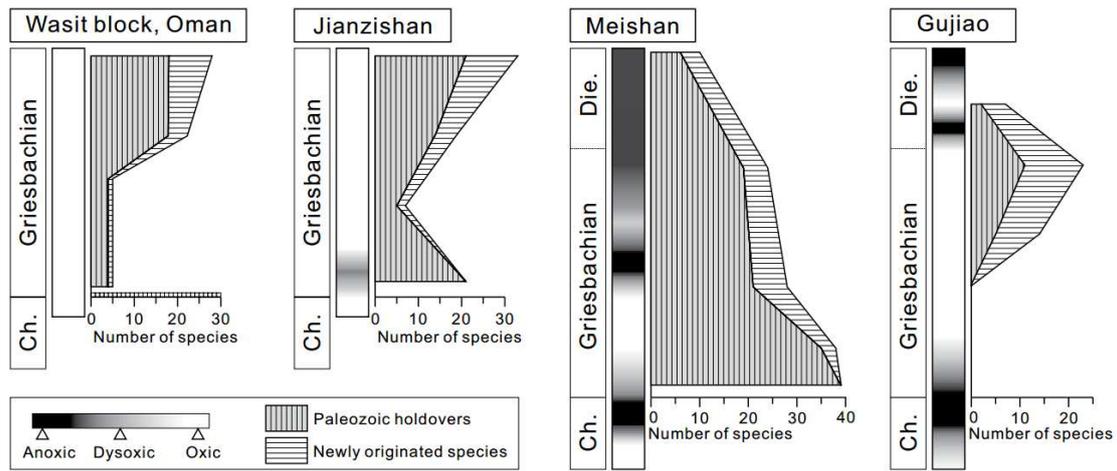
Figure 15. Correlation of paleoredox conditions and taxonomic richness of Paleozoic holdovers and new originated species. The redox conditions of Wasit block, Oman is from Clarkson et al. (2016) and the paleontological data are from Twitchett et al. (2004). The redox conditions of Meishan is from Chen et al. (2014) and Li et al. (2016) and the paleontological data is from Chen et al. (2007) and Song et al. (2013). Ch. Changhsingian; Die. Dienerian.